CONTENTS

CONTENTS
(continued)

LIST OF TABLES

LIST OF TABLES
(continued)

LIST OF FIGURES

LIST OF FIGURES
(continued)

Decay Studies of a Long Lived High Spin Isomer of ^{210}Bi

Dale Glenn Tuggle

Lawrence Berkeley Laboratory
University of California
Berkeley, CA 94720

Abstract

A source of ≈30 μg of pure (> 90%) ^{210m}Bi ($t_{1/2}$=9·) was prepared by irradiating ^{209}Bi in a nuclear reactor. After chemical separations to remove ^{210}Po from the irradiated bismuth sample were completed, the ^{210}Bi was electromagnetically separated from the ^{209}Bi by a series of two isotope separations to create the source mentioned above. This source was then used to conduct alpha, conversion electron, gamma, gamma-gamma coincidence, and alpha-gamma coincidence spectroscopic studies of the decay of ^{210m}Bi. The partial half life for the alpha decay of ^{210m}Bi was measured as 3.0×10^{6}yr. A lower limit of 10^{13} years was set for the partial half life for the decay of ^{210m}Bi to ^{210}Po. Alpha decay of ^{210m}Bi to 8 excited states of ^{206}Tl was observed. A lower limit of 10^{-6}% was set for the branching ratio of the parity forbidden alpha decay of ^{210}Bi to the ^{206}Ti ground state. Theoretical decay rates for the alpha decays of ^{210m}Bi, ^{210}Bi, ^{211}Po, and ^{211m}Po were calculated using the method developed by Hans Mang. A comparison of the calculated and experimentally measured alpha decay rates of ^{210m}Bi showed good agreement for the relative alpha decay rates.

Acknowledgments

I wish to thank my research director, Professor Isadore Perlman, and Dr. Frank Asaro for their guidance and support throughout the course of this work.

I am grateful to Helen Michel and James Harris for their assistance in the chemical separations and to Duane Mosier and Ed Arnold who maintained the electronics equipment.

For his guidance during the isotope separations I am indebted to Dr. Maynard Michel. The construction of the ^{210m}Bi collector system for the isotope separator was a difficult task because of its small size and I am grateful to Dick Escobales and G. G. Young for accomplishing the task.

My greatest appreciation is for my wife, Jeanette, whose encouragement, support, and patience kept my spirits up even during the difficult times.

My parents also deserve a note of thanks for their support and interest.

Work performed under the auspices of the U. S. Energy Research and Development Administration.

I. Introduction

The problem of obtaining exact nuclear wave functions which could be used to calculate nuclear properties is extremely complex for all but the simplest nuclear systems (^1H,^2H). Approximate nuclear wave functions, however, can be determined using various approximations for the forces in a nucleus and these approximate wave functions can be used with moderate success to calculate nuclear properties. The description of a nucleus in terms of some set of approximate wave functions is called a model. Some of the models which have been used successfully to calculate nuclear properties are the Liquid Drop Model, the Shell Model, and the Collective Model. Descriptions and discussions of these models as well as several others can be found in many places.[1] This work is concerned with the Shell Model because of its prediction of closed nucleon shells at N or Z = 2, 8, 20, 28, 50, 82, 126.

The isotope ^{210}Bi has 83 protons which is one more than the number needed for a closed shell at Z = 82, and 127 neutrons which is one more than the number needed for a closed shell at N = 126. In this region near a closed neutron and a closed proton shell the description of a nucleus in terms of shell model wave functions is expected to be good, and in addition the calculation of nuclear properties is simplified because it is not necessary to use coefficients of fractional parentage.

The specific nuclear property of ^{210m}Bi of concern in this work

was its rate of alpha decay to states of ^{206}Tl. A method for calculating alpha decay rates of nuclei using shell model wave functions was developed by Hans Mang[2-5]. The purpose of this work was to measure experimentally the alpha decay rates of ^{210m}Bi to various states of ^{206}Tl and to also calculate for comparison these same alpha decay rates using Mang's method.

This report is consequently divided into three major parts. The first discusses the method of preparation of ^{210m}Bi counting sources and the results of spectroscopic measurements using these sources. The sources were made by electromagnetic separation of ^{210m}Bi out of a chemically purified sample of irradiated ^{209}Bi. Alpha, gamma, conversion electron, gamma-gamma coincidence, and alpha-gamma coincidence spectra of ^{210m}Bi were recorded using these sources. The second part explains the exact calculational method used to calculate alpha decay rates and discusses the results of calculations of the alpha decay rate for the nuclei ^{211}Po, ^{211m}Po, ^{213}Bi, and ^{213m}Bi.

The third section is a summary of the experimental data used to produce a decay scheme for ^{210m}Bi and an energy level diagram of ^{206}Tl. The experimental alpha decay rates are compared to the values calculated using different configuration mixing schemes for ^{206}Tl.

II. Experimental Measurements

A. Preparation of ^{210m}Bi Sources

1. ^{210m}Bi Production

Although there are several target projectile reactions that can produce ^{210m}Bi, the neutron capture reaction of ^{209}Bi was chosen because

of its simplicity and the ability to produce milligram quantities of ^{210m}Bi. The main difficulty with this production method is that the ^{210m}Bi must be electromagnetically separated from the ^{209}Bi target to produce a source with a suitable specific activity ($> 10^3$d/min-μg). Previous studies[6-12] of the decay of ^{210m}Bi used sources with specific activities of less than 30 d/min-μg, and consequently were not able to observe alpha transitions with branching ratios less than 0.1%.

A 10 gram target of ^{209}Bi was placed in the Savannah River Reactor Facility where it was exposed to a neutron flux of approximately 10^{15} neutrons/cm^2- second for a period of about one year. The neutron capture cross section of ^{209}Bi to yield ^{210m}Bi has been measured as 19±2 millibarns.[13] Using this cross section value and the approximate flux and length of irradiation, the expected yield of ^{210m}Bi was calculated as 60 milligrams.

Table 1. ^{209}Bi(n,γ)X Reactions

^{209}Bi (n,γ) ^{210}Bi (ground state)	$\sigma_c \approx 14\pm3$ mb[a]
^{209}Bi (n,2n) ^{208}Bi	$\sigma(E_n > 8$ MeV) ≈ 1.3 mb[b]
^{208}Bi (n,2n) ^{207}Bi	$\sigma(E_n > 8$ MeV) ≈ 2.9 mb[b]
^{209}Bi (n,3n) ^{207}Bi	$\sigma \approx 2.2 \times 10^4$ mb[b]

(a) Ref. 13
(b) Ref. 14

The production of the ground state of ^{210}Bi posed no problem since ^{210}Bi(g.s.) beta decays with a half life of 5.01 days[15] to ^{210}Po. The ^{210}Po which was produced in the ^{209}Bi target was removed by chemical separations which will be discussed in the next section. Both ^{207}Bi and ^{208}Bi, which were produced in the ^{209}Bi target, decay by electron capture and did not cause any problems in recording the alpha decay spectrum of ^{210m}Bi, but the gamma rays produced following ^{207}Bi and ^{208}Bi electron capture decay interfered with measurements of the gamma spectrum produced by the alpha decay of ^{210m}Bi to excited states of ^{206}Tl and the subsequent gamma decay of these excited states to other lower energy excited states or to the ^{206}Tl ground state. Note that ^{207}Bi can be produced from ^{209}Bi by either two consecutive (n,2n) reactions or one (n,3n) reaction. Eastwood and Roy[14] calculated the rate of production of ^{207}Bi for each of these reaction paths. A comparison of their calculated rates to the experimentally measured rate led them to the conclusion that the reaction (n,3n) is primarily responsible for the production of ^{207}Bi in a ^{209}Bi target exposed to a fast (> 8 MeV) neutron flux.

The ^{209}Bi sample also contained a small amount of Sb. Gamma spectra taken using the irradiated bismuth sample prior to any electromagnetic separations showed gamma peaks with energies and intensities corresponding to those of ^{125}Sb ($t_{\frac{1}{2}}$ = 2.7 yr).[15] This isotope was probably produced by two consecutive (n,γ) reactions

^{123}Sb (n,γ) ^{124}Sb $\qquad\qquad$ σ_c = 3.3b [15]

^{124}Sb (n,γ) ^{125}Sb $\qquad\qquad$ σ_c = 2000 [15]

Because of the much shorter half life for the decay of ^{125}Sb as compared to ^{210m}Bi and the much larger neutron capture cross sections of ^{123}Sb

and ^{124}Sb as compared to ^{209}Bi only trace amounts ($< 10^{9}$ atom %) of ^{123}Sb in the original ^{209}Bi sample caused peaks to occur in the gamma spectrum that had intensities of the same order of magnitude as the intensities of the ^{210m}Bi gamma peaks.

The removal of these impurities from the sample (^{207}Bi, ^{208}Bi, ^{210}Po, and ^{125}Sb) and of ^{210m}Bi from ^{209}Bi are the topics of the next two sections. Both chemical and electromagnetic techniques were used.

2. Chemical Removal of ^{210}Po

As mentioned in the preceding section the beta decay of the ^{210}Bi ground state produces ^{210}Po which decays by alpha particle emission to ^{206}Pb with a half life of 138.4[15] days. The ^{210}Po was separated out of the irradiated bismuth sample for several reasons. One was to reduce the total alpha activity of the sample to facilitate its handling and shipping. During the irradiation approximately equal amounts of ^{210}Po (Daughter of ^{210}Bi) and ^{210m}Bi were produced but the alpha activity of the ^{210}Po was much higher (six orders of magnitude) than for ^{210m}Bi because of its much shorter half life. Another reason for removing ^{210}Po from the sample was that it produced a high background alpha counting rate in the energy region of the alpha spectrum where ^{210m}Bi alpha peaks occur. And finally, one part of this project was to search for the decay of ^{210m}Bi to ^{210}Po, by reducing the amount of ^{210}Po in the sample to a low level and then monitoring the increase in ^{210}Po alpha activity as ^{210}Po was produced by the decay of ^{210m}Bi to ^{210}Po.

The separation of ^{210}Po out of the sample was accomplished by distillation and solvent extraction. The distillation which removed the bulk of the ^{210}Po was done at Savannah River Reactor Facility several

weeks after the end of the irradiation. The boiling points for Po and Bi metal are

Po - 962°C [16]

Bi - 1562°C [16]

The Bi metal sample was then shipped to Lawrence Berkeley Laboratory where it was eventually dissolved by reacting it with concentrated nitric acid. A small amount of this solution was diluted and was used to make an alpha source by electrodeposition on a Pt plate. An alpha spectrum was taken using a Frisch grid chamber. The spectrum is shown in Fig. 1a. The ratio of ^{210m}Bi alpha counts to ^{210}Po alpha counts calculated by summing over the channel limits shown in Fig. 1a was 0.29.

To reduce the amount of ^{210}Po further the bismuth sample was dissolved in 160 ml of 4M HNO_3 solution and the solution was divided into 4 portions of ~40 ml. Then solvent extractions with 40 ml fractions of dibutyl carbitol[17] were performed to remove ^{210}Po from the aqueous solutions. An alpha spectrum of a source made using a portion of the aqueous phase after the extraction is shown in Fig. 1b. The ratio of ^{210}Po counts to ^{210m}Bi counts was .097. The extraction had reduced the ratio by a factor of 3. A second extraction produced a further reduction of the ^{210}Po/^{210m}Bi alpha count ratio by a factor of 4.7.

Two extractions were performed on each of the four portions of the 4M HNO_3 solution and a comparison of alpha spectra showed that in each case the ^{210}Po/^{210m}Bi count ratio was reduced by a factor of 3 to 5 per extraction. After completing the extractions three of the four aqueous solutions were mixed together and shipped to Oak Ridge National Laboratory where an electromagnetic separation was conducted. The fourth

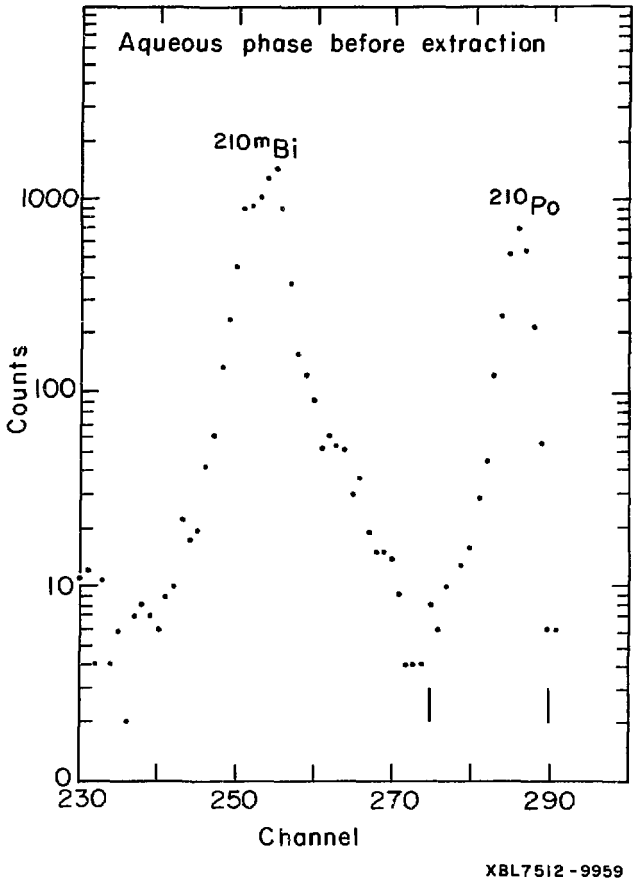

Figure 1a. Alpha spectrum before one dibutyl carbitol extraction.

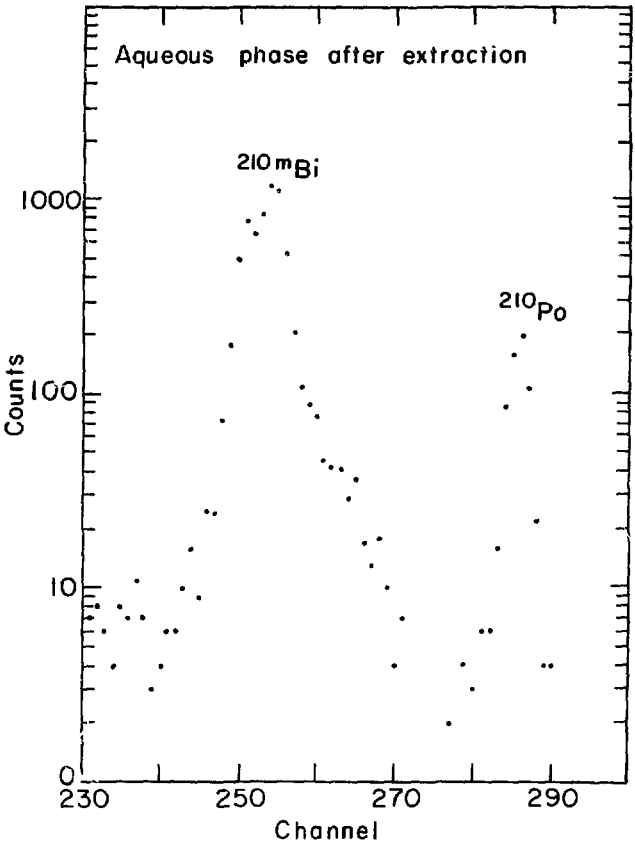

XBL7512-9956

Figure 1b. Alpha spectrum after one dibutyl carbitol extraction.

portion was used to prepare alpha counting sources used in measuring the half life of ^{210m}Bi and to conduct some trial runs on the electromagnetic isotope separator at Lawrence Berkeley Lab. The average Po/Bi ratio of alpha counts for all four samples was 0.03.

This Po/Bi ratio was reduced even further in the electromagnetic isotope separations. The exact mechanism for that separation was not investigated but since ^{210}Po and ^{210m}Bi have approximately the same mass, the separation is not due to electromagnetic effects but to some difference in the physical properties of ^{210}Po and ^{210m}Bi which causes them to be ionized at different rates in the ion source of the separator.

3. Electromagnetic Isotope Separation

After chemical separation to remove ^{210}Po from the sample had been completed, a mass analysis of the sample was conducted and the amount of ^{210m}Bi in the sample was measured as 0.130±.005 atom % of the total bismuth. A comparison of the ^{210}Po to the ^{210m}Bi alpha decay rates was then used to calculate the amount of ^{210}Po in the sample as 4 x 10^{-3} atom %. And by comparing gamma ray intensities the amounts of ^{207}Bi, ^{208}Bi, and ^{125}Sb were calculated as 10^{-5} atom %, 5 x 10^{-3} atom %, and 10^{-6} atom % respectively.

By an electrodeposition technique which is discussed in Section B1, sources for alpha spectroscopy were prepared and used to measure the half life of ^{210m}Bi. But these sources were not suitable for later experiments because of their low counting rates. In order to achieve adequate energy resolution (< 50 keV FWHM) for an alpha spectrum, the thickness of the source had to be kept to a thickness of less than 500 μg/cm^2 of bismuth. Because 99.99 atom % of the sample was ^{209}Bi, a 1 cm^2 area source with a thickness of 500 μg/cm^2 would have

contained only .65 μg of ^{210m}Bi and a ^{210m}Bi alpha activity of ~700 d/min. Since thicker sources would decrease the resolution of the alpha spectrum, the only way to get sources with higher count rates was to use an electromagnetic isotope separator to separate ^{210m}Bi away from the ^{209}Bi. Electromagnetic separations would also separate ^{210m}Bi from ^{207}Bi, ^{208}Bi, ^{125}Sb, and thus reduce the background gamma counting level in sources made with separated material.

The separation of ^{210m}Bi was done in two stages. First a 7 gram portion of the 0.13 atom % ^{210m}Bi sample was run through the Calutron at Oak Ridge National Lab. The material collected as output from that run was then used as input into the isotope separator at Lawrence Berkeley Lab and the output of that run was collected on an Al foil which was then used as a source for spectrographic measurements. These separations are discussed in more detail in the next few paragraphs.

The amount of bismuth sent to Oak Ridge National Laboratory was measured by running an EDTA titration with pyrocatinal violet as an indicator on a small fraction of the sample solution. The total bismuth content of the sample was measured as 4.5 grams. This sample was run through the Calutron and the ^{210m}Bi fraction collected on a 5 mil copper foil. The efficiency of the run, as measured by integration of the ^{209}Bi beam current, was 5%. Correspondingly the amount of ^{210m}Bi that should have been collected was calculated as 0.28 mg.

It was assumed that the efficiency of the runs to be conducted at Lawrence Berkeley Lab would also be ~5% and an estimate of the final amount of ^{210m}Bi that would be collected was made as shown below.

$$0.28 \text{ mg } ^{210m}\text{Bi} \times .05 = 14 \text{ μg } ^{210m}\text{Bi}$$

This amount of ^{210m}Bi would have an alpha activity of ~20,000 d/min. This amount of activity is low so the decision was made to do two things to increase it. First another 2 grams of bismuth (.13% atom % ^{210m}Bi) was sent to Oak Ridge National Lab. And second, the ion source from the first Oak Ridge National Lab run was washed to recover the bismuth. This recovered bismuth was added to the 2 gram sample and a second separation run was made.

The copper collector foils from both runs were shipped to Lawrence Berkeley Lab where they were dissolved in a 6M HCl - .1M HNO_3 solution. The targets also contained some sputtered graphite which was filtered out of the acid solution and placed in a platinum boat. The graphite was then burned, the Pt boat rinsed with concentrated nitric acid, and the rinse solution added to the original solution.

The solution was taken to dryness, dissolved in 50 ml of 1M HCl, and diluted to 500 ml causing Bi to precipitate as BiOCl. The solubility of BiOCl in .35M HCl at 25°C has been measured as 1.3 mg/1000 gm H_2O [18] and should be significantly lower for .1M HCl and ~20°C. The total amount of Bismuth was estimated at 30 mg (^{210m}Bi~2% based on an enrichment factor of ~20 for the Calutron) of which < 3% remains in solution while the rest precipitates.

The BiOCl precipitate was filtered and washed with .01M HCl. Then it was dissolved in 50 ml of 1M HCl. By adding 15 mg of powdered zinc to the solution the bismuth was reduced and precipitated as the metal, which when filtered and washed was used as input material for the isotope separation done at Lawrence Berkeley Lab. The amount of Bi metal collected was 26.9 mg. The ratio of ^{210m}Bi/^{209}Bi was measured as 2%. Using

these values an overall efficiency for the separation runs at Oak Ridge National Lab was calculated as 7%.

The electromagnetic isotope separator at Lawrence Berkeley Laboratory was constructed in the mid 1960's.[19] It is similar in design to the Scandinavian separators of the 1950's but with some modifications and improvements. The overall layout of the machine is shown in Fig. 2. Only the first stage of the machine is currently in use. The machine has a 90° deflection with a radius of curvature of 152.4 cm and a total beam path of 4.82 m. The base pressure of the vacuum system is 10^{-5} torr except in the ion source which has a base pressure of 2×10^{-6} torr.

A diagram of the ion source used for solids is shown in Fig. 3a and a closer view of the source oven is shown in Fig. 3b. The temperature of the oven is raised by passing a current through it until the vapor pressure of the sample becomes high enough that enough material diffuses into the source chamber to support a plasma.

The bismuth samples were loaded into the oven in two ways. In the initial series of trial runs using input material that had not been isotope separated at Oak Ridge National Lab, .001 ml volumes of a 4M HNO_3 solution which had a bismuth concentration of 6.4 mg/ml were placed on a platinum foil and taken to dryness. The platinum foil was then folded around the sample and this package of bismuth wrapped in Pt foil was placed in the oven of the isotope separator.

In the series of isotope separation runs which used as input material the bismuth which had undergone an isotope separation at Oak Ridge National Lab, weighed amounts of powdered bismuth metal were placed directly into the oven. This powdered bismuth was obtained by

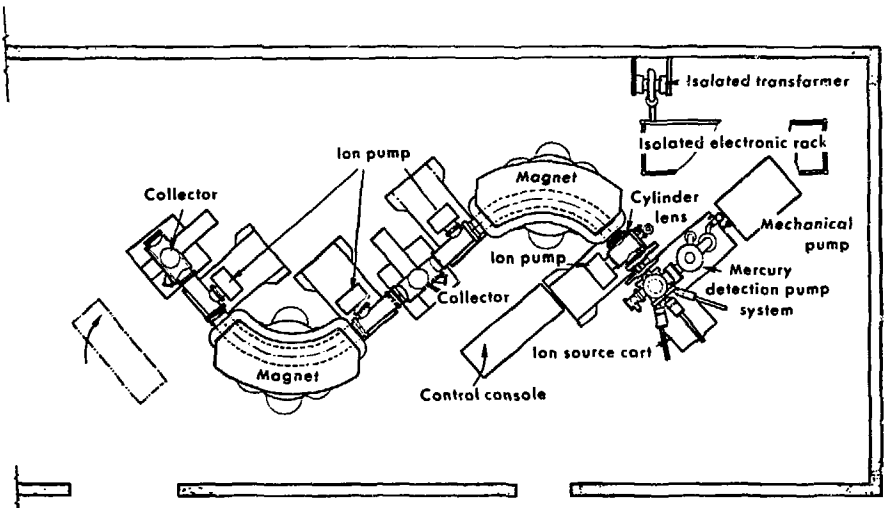

Figure 2. Overall layout of cascade isotope separator.

XBL7512 - 9963

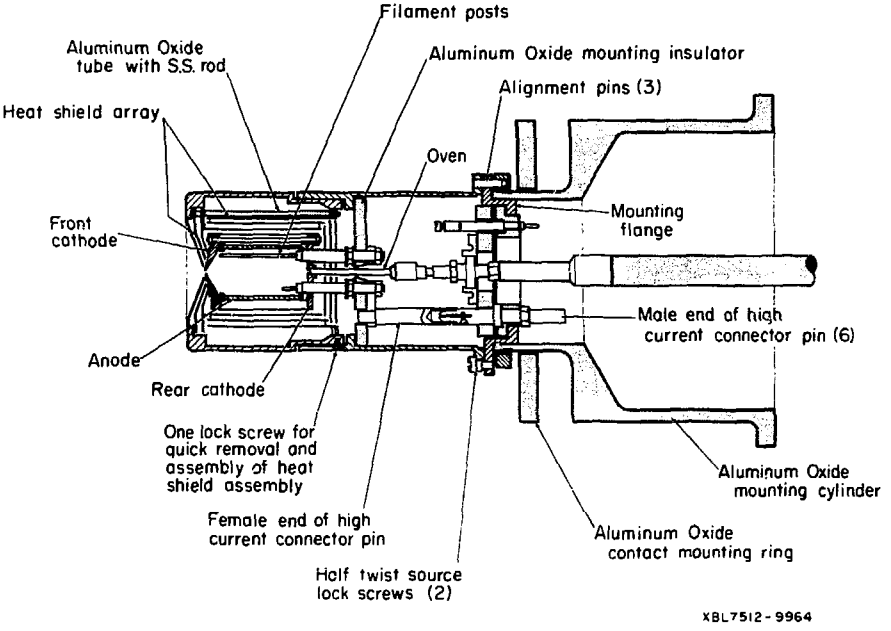

Figure 3a. Isotope separator ion source.

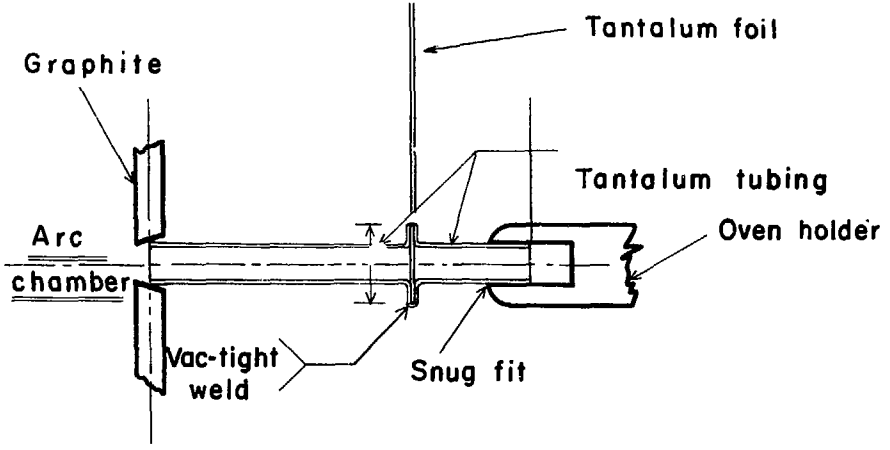

Figure 3b. Isotope separator directly heated source oven

XBL7512-9962

methods described earlier in this section. A problem with loading powdered metal into the isotope separator ion source oven was that some powder stuck to the walls of the oven. This material on the walls of the oven probably vaporized during start-up and tuning operations when the separated isotope beams were not being collected. Consequently the efficiency for the runs was reduced.

The collector system for the isotope separator is mounted on a differentially pumped vacuum probe[20] which allows the collector system to be removed without significantly disturbing the vacuum within the separator. The collector housing itself, shown in Fig. 4, is a rectangular box with two sides open. One end of the housing fits onto the vacuum probe and into the other end which is open a set of rectangular plates can be fitted. The plates fit into aluminum oxide slots along the top and bottom of the housing and when completely in place make electrical contact with a connector at the closed end of the housing. The surfaces of these plates are placed perpendicular to the beam direction when collecting the isotope beams.

The advantage of using a series of plates is the ease of assembly and disassembly of a collector system. The electrical connections with the plates serve several purposes. First the amount of beam current striking a particular plate can be measured to determine beam intensity. This intensity can then be integrated over the course of a run and used to determine the amount of material collected (or at least the amount of material which struck the collector). Secondly, by applying a negative voltage to the plate just preceding the one on which beam intensity if being measured, electrons scattered when

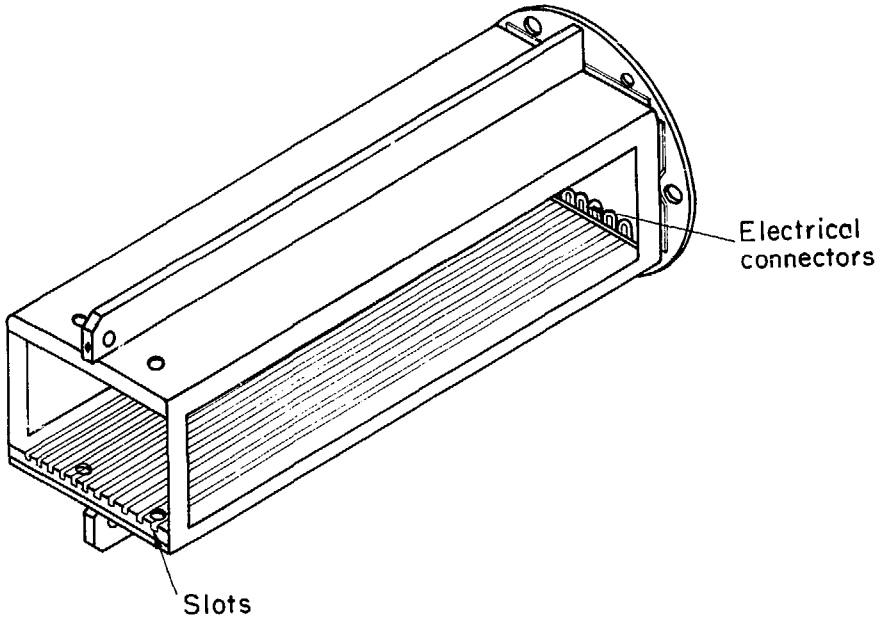

XBL7512-9954

Figure 4. Isotope Collector System Housing

the beam strikes the collecting plate can be kept from escaping the plate. The loss of electrons from the collecting plate causes readings of beam intensity to be too high.

For the collection of ^{210m}Bi a special set of collector plates was constructed so that the ^{210m}Bi could be collected on an aluminum foil which could be used as a source for spectrographic measurements.

Collection of the ^{210m}Bi beam directly onto the foil was not feasible because sputtering limited the amount of ^{210m}Bi that could be collected to a few $\mu g/cm^2$. After collecting that amount of ^{210m}Bi an equilibrium was reached where one ^{210m}Bi atom was knocked off of the collecting foil by each incoming 40 keV ^{210m}Bi ion. The self sputtering ratio (atoms sputtered/incident ion) of ^{210m}Bi has never been measured but an estimate of 54 was made by extrapolating from the values of platinum and lead which are 52 and 53[21] respectively for incident ion energies of 45 keV. The total amount of ^{210m}Bi to be collected was ~30 μg which would give a thickness of 60 $\mu g/cm^2$ when spread over a collection area of .5 cm^2.

One method of increasing the amount of ^{210m}Bi which can be collected on a foil is to decelerate the ^{210m}Bi ions before they strike the foil to an energy of ~1 keV by using a retarding potential. This method was used by Sheline[22] to prepare ^{210m}Bi targets for use as targets in accelerator experiments. The difficulty with this method is to maintain the beam focus in spite of irregularities in the deceleration field and the increased effect of space charge blow-up.

The problem of collecting ^{210m}Bi at thicknesses of ~60 $\mu g/cm^2$ was solved in this work by letting the beam strike a Be foil and collecting the sputtered material. A diagram of the collector designed to

accomplish this is shown in Fig. 5. A Be foil target was mounted at an angle of 30° to the beam direction and a curved (3 mm radius) piece of 3 mil Al foil was placed above the Be foil to catch the material sputtered by the beam. A slit was cut into the Al foil to allow the beam to pass through it. Although some of the sputtered material escapes back out of this same slit through which the beam entered, the amount was less than 3%. This is due to the fact that sputtering at an incident ion energy of 40 keV is highest in intensity in the direction perpendicular to the Be foil.[21] The intensity as the angle to the perpendicular increases is proportional to the cosine of the angle to the perpendicular. This cosine distribution can be seen in Fig. 6 which is a picture of the Al foil used in the ^{210m}Bi separation runs. This foil, which had an average thickness of ~80 μg/cm^2 and a total alpha activity of 5 x 10^4 d/min was used as a counting source for many of the spectroscopic measurements discussed in this work.

One final aspect of the ^{210m}Bi electromagnetic separation is efficiency. There are many factors that can affect the efficiency and it is not the purpose of this report to try to explain them. Instead the efficiency results for the various bismuth separation runs will be presented. Preliminary runs on the isotope separator were conducted with natural bismuth metal and with Bi nitrates which were wrapped in platinum foil as discussed earlier in this section. The nitrate runs were repeated with irradiated bismuth samples (0.13% ^{210m}Bi). And the bismuth which had been separated at Oak Ridge National Lab (2% ^{210m}Bi) was run as powdered bismuth metal.

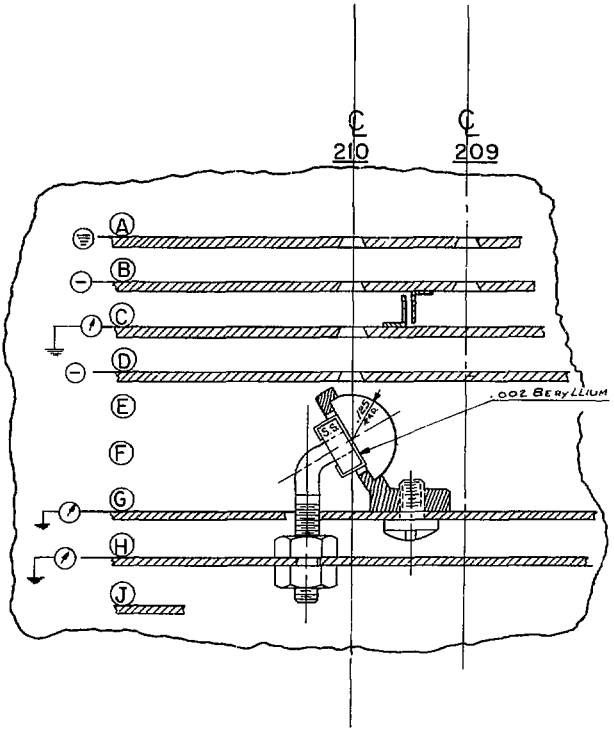

Figure 5. PLAN VIEW THRU COLLECTION BOX

Scale: (4 Times Size)

XBL761 - 2139

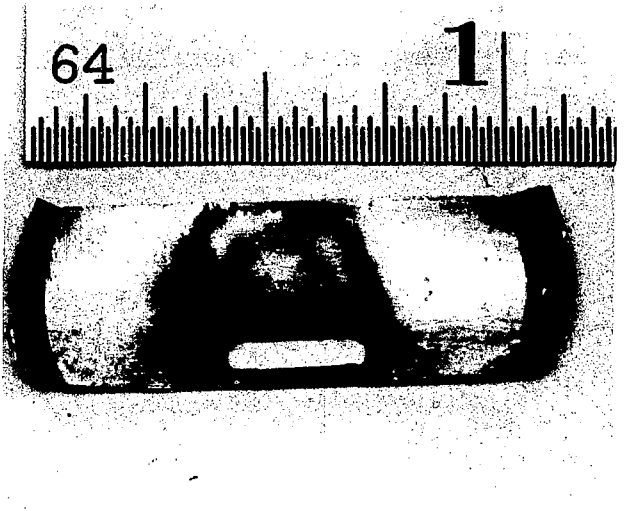

XBB 7510-8970

Figure 6. ^{210m}Bi collector foil.

Table 2. Isotope Separator Efficiency Measurements

Input Form Natural Bismuth Runs	Amt (Bi)	Av Beam Current (^{209}Bi)	Eff	
Metal	2 mg	3 μA	8 %	
Bi nitrate in Pt foil	1 mg	1 μA	8.6 %	
	2 mg	4 μA	7.0 %	
	1.3 mg	3 μA	3.5 %	
Irradiated Bismuth Runs (.13% ^{210m}Bi)				
Bismuth nitrate in Pt foil	5 mg	4 μa	8.7 %	
	5 mg	7 μa	4.3 %	(a)
	5 mg	3 μa	3.9 %	(b)
	6.6 mg	5 μa	8.0 %	
Irradiated Bismuth Runs (2 % ^{210m}Bi)				
Sample Form Metal Powder	3.7 mg	2 μA	10.2 %	
	4.1 mg	3 μA	14 %	
	3.7 mg	4 μA	11.3 %	
	3.4 mg	4 μA	5.5 %	(c)
	4.45mg	3 μA	13.5 %	
Overall Collection Efficiency for ^{210m}Bi (2% ^{210m}Bi)			12.2 %	

(a) Machine failure during the run is partly responsible for the lower value.

(b) Sparking between ion source and extractor forced early shutdown of the machine.

(c) Oven dropped after loading and some material lost.

B. Spectroscopic Measurements

The ultimate purpose of obtaining a sample of ^{210m}Bi was to observe spectroscopically its decay and to compare the data derived from these observations with calculated decay rates. It is the purpose of this section to describe both the methods and results of various spectroscopic measurements on the long lived isomer of ^{210}Bi. The division of this section into parts is based on types of spectroscopy, e.g. alpha or gamma, or conversion electron. All of these measurements are used together in Chapter IV to show the decay characteristics of ^{210m}Bi and to compare them to theory.

1. Alpha Singles

The alpha spectroscopic measurements made on ^{210m}Bi can be divided into three groups each addressing a different problem and using a particular set of experimental parameters. One group of measurements was done to determine the half life of ^{210m}Bi. Another group of measurements was aimed at measuring the approach to equilibrium of the ^{210}Po/^{210m}Bi alpha counting ratio and thus determining the beta decay (or possibly gamma) decay rate for ^{210m}Bi. And finally a third group of measurements was taken to measure the branching ratios and energies of ^{210m}Bi alpha decays to states in ^{206}Tl. Each of these three groups of measurements will be discussed separately in the next three sections.

a. ^{210m}Bi Half Life

The alpha decay half life of ^{210m}Bi was determined by measuring the alpha activity of a source containing a known amount of the isomer. Only the alpha decay rate of ^{210m}Bi was used for calculation of the half life of ^{210m}Bi because the rates for other decay modes of ^{210m}Bi are at least six orders of magnitude smaller than the alpha decay rate. The value for the half life found using this method was $3.04 \pm .06 \times 10^6$ yr. which is

is somewhat lower than the value $3.55 \pm .12 \times 10^6$ found by Lange and Hagee[23] using a similar technique.

Sources for this half life determination were made from a solution of the irradiated bismuth target after chemical separations to remove ^{210}Po had been completed but before any electromagnetic separations had been started. This solution was mass analyzed using a mass spectrometer and found to contain 0.150±.005% ^{210m}Bi. To measure the total bismuth concentration of the solution 1 ml portions were withdrawn from the solution which had a total volume of ≈100 ml. These 1 ml samples were diluted to 10 ml and titrated with a .05 M diNa EDTA solution using pyrocatinol violet as an indicator. The bismuth concentration was found to be 6.8±.1 mg/ml.

Sources were prepared from this solution by an electrodeposition technique. A small volume (20 λ)of the bismuth solution was placed on a Pt plate which served as the cathode in the electrodeposition cell. A diagram of the apparatus is shown in Fig. 7. After placing the Pt plate in the electrodeposition cell the 20 λ solution was diluted to 1-2 ml. This solution was held in the cell by maintaining a slight negative pressure in the cell. A current of 50 milliamps was passed through the cell for 10 minutes causing the bismuth to deposit on the Pt plate (probably as bismuth hydroxide but investigations were not conducted to determine this). After 10 minutes the liquid was rapidly removed from the cell without turning off the potential across the electrodes.

To get valid half life measurements this electrodeposition had to be quantitative. The effectiveness of the deposition was monitored by rinsing the cell with 4 MHNO_3, adding this rinse to the original cell solution, and taking this solution to dryness on a Pt plate. This plate was then placed in a grid chamber and alpha counted. If this plate

Electrodeposition cell

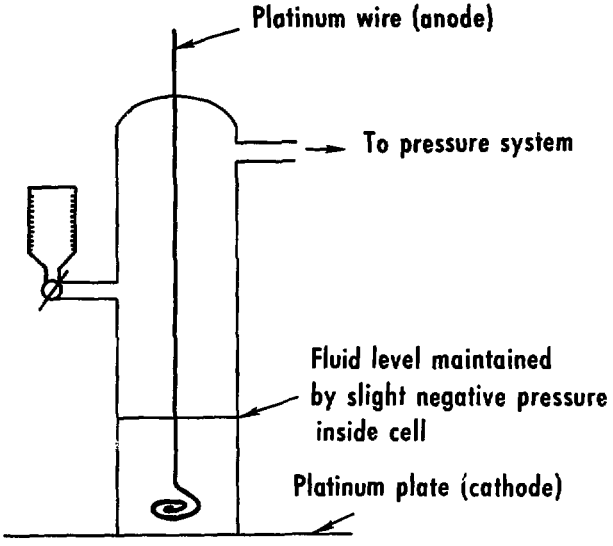

XBL7512-9960

Figure 7. Electrodeposition cell.

showed any alpha activity the run was discarded.

The sources made by electrodeposition were alpha counted in a Frisch grid chamber using a gas mixture of 90% Ar 10% methane at a pressure of 8 lb/in and a flow rate through the chamber of 30 cc/min. A collimator 3.17 mm in height and 26.95 mm in diameter was used to improve the resolution of the spectra. The efficiency with the collimator was calculated by assuming a constant density distribution of the bismuth in a 7 mm diameter circle and integrating numerically over all points within the circle. The overall efficiency of the chamber using this calculation was 37.3%. Table 3 shows the values measured for the half life and some of the parameters for those measurements.

Table 3. Half Life of ^{210m}Bi

Amt ^{210m}Bi	d/min	$t_{\frac{1}{2}}$ (10^6 yr)
(2.2±.1) x 10^{-3}μg	2.73±.04	3.05±.15
(2.21±.1) x 10^{-3}μg	2.98±.04	2.80±.14
(2.21±.1) x 10^{-3}μg	2.83±.04	2.94±.15
0.167±.005μg	208±1	3.04±.06

b. ^{210m}Bi Decay to ^{210}Po

The decay of ^{210m}Bi to ^{210}Po is possible through several paths as shown in Fig. 7.5. The isomeric state of ^{210}Bi can decay by gamma emission to the ground state which can then beta decay to form ^{210}Po. Or the isomeric state can beta decay to the ground state of ^{210}Po or to either of the first two excited states of ^{210}Po.

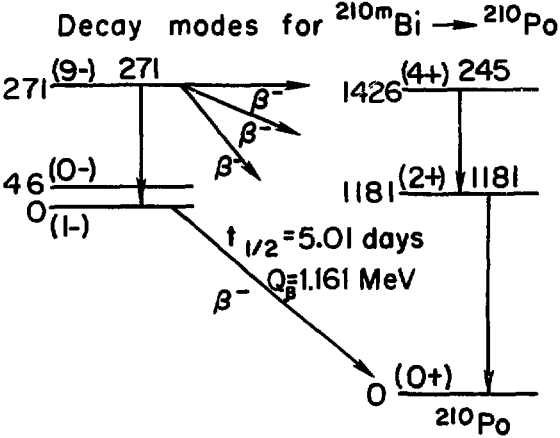

Figure 7.5. Decay modes for the decay of ^{210m}Bi to ^{210}Po.

All of these possible decay modes should be highly hindered by the large angular momentum changes involved. The partial half life of the gamma transition (E8) between the isomeric and the ground state of ^{210}Bi was estimated as 5.5 x 10^{20} yr. using the Weisskopf formula shown below[24]:

$$t_{\frac{1}{2}} = \frac{693 \times .645 \times 10^{21}}{S} \left(\frac{140}{E(MeV)}\right)^{2L+1} A^{2/3L} \text{ sec}$$

$$S = 2\,[1+(1/L)]\,/\left\{[(2L+1)\cdot(2L-1)\cdot\ldots\cdot 5\times 3\times 1]\,[1+(L/3)]\right\}^2$$

Beta decay to the first three states of ^{210}Po involves angular momentum changes of 9, 7, and 5 respectively. Because of these large angular momentum changes it is expected that all of these beta decays will have a log ft > 20. Using a log ft = 20 as a lower limit for the beta transitions to all three levels of ^{210}Po estimates of the partial beta decay half lives shown in Table 4 were made by extrapolating the tables in reference 15. These values are expected to be minimums for the half life.

Table 4. Minimum Beta Decay Half Lives for ^{210m}Bi

^{210}Po level (keV)	Spin, Parity	Qp (keV)	$t_{\frac{1}{2}}$ (yr) (a)
0	0+	1432	10^{13}
1181	2+	251	10^{15}
1426	4+	6	10^{20}

(a) log ft = 20

Based on these estimates for the minimum partial half lifes of the various

decay modes of ^{210m}Bi to ^{210}Po, the assumption can be made that the decay of ^{210m}Bi to ^{210}Po has a maximum branching ratio of less than 3×10^{-5}%. But Levy and Perlman[11] experimentally measured this branching ratio as 3.7×10^{-3} by observing the growth of ^{210}Po in a sample of bismuth (~10^{-2}% ^{210m}Bi) which had been purified of ^{210}Po. Because no direct observation of the decay of ^{210m}Bi to ^{210}Po was made, the mode of the decay was not determined.

The decay rate of ^{210m}Bi to ^{210}Po was also measured by Rusinov[7] by comparing the alpha decay rate of ^{210m}Bi to ^{210}Po. The ratio of the ^{210}Po to ^{210m}Bi alpha decay rate was checked over three half lives of ^{210}Po ($t_{\frac{1}{2}}$ = 138.4 days) and found to be constant at 5×10^{-6}. Using the value 3.04×10^{6} yr. for the half life of ^{210m}Bi and assuming that the decay of ^{210m}Bi to ^{210}Po was at equilibrium during the measurements, the partial halflife for the decay of ^{210m}Bi to ^{210}Po can be calculated as 6×10^{10} yr., a value several orders of magnitude lower than any of the predicted half lives. Rusinov made this measurement with a bismuth source having a specific alpha activity of 14 d/min-μg, whereas the source produced by the final isotope separation in this work had a specific alpha activity of 1.2×10^{3} d/min-μg.

Using this source the alpha decay ratio of ^{210m}Bi to ^{210}Po was measured. The ratio was initially found to be $\leq 1 \times 10^{-6}$ but measurements taken slightly less than one year later with an order of magnitude more counts gave a value of $2.8 \pm .6 \times 10^{-7}$.

This decrease in the ratio of the ^{210}Po to ^{210m}Bi alpha decay rate corresponds to the decrease expected if only the decay of ^{210}Po is considered. This indicates that the rate of production of ^{210}Po in the sample was much slower than its rate of decay, and from these measurements only a lower limit for the partial half life for the decay of ^{210m}Bi to

^{210}Po can be determined. This lower limit is $1.0 \pm .3 \times 10^{13}$ years which is several orders of magnitude higher than the partial half life calculated using Rusinov's data.

The measurements of the ratio of the ^{210}Po to ^{210m}Bi alpha decay rate was made using a solid state silicon gold surface barrier detector with a diameter of 6 mm. The detector was placed within 2 mm of the source to maximize the efficiency of the system. The pressure in the counting chamber was maintained at ~15 microns by a mechanical pump trapped with dry ice and alcohol. The resolution of the system was 40 keV because the small distance between the source and the detector increased the effect of self absorption in the source.

c. ^{210m}Bi Decay to ^{206}Tl

Alpha decay was observed in the alpha singles spectrum of ^{210m}Bi to six excited states of ^{206}Tl, as seen in Fig. 20. But no alpha decay of ^{210m}Bi to the ground state of ^{206}Tl was seen despite special efforts to search for the decay which had been reported by reference 6.

An alpha spectrum of a ^{210m}Bi source is shown in Fig. 8. This spectrum was taken using a solid state 150 mm^2 active area silicon gold surfact barrier detector with a resolution of 32 keV FWHM at room temperature.

The counting chamber used was designed to prevent internal conversion electrons from reaching the detector and creating peaks in the spectrum having an energy equal to the sum of the energy of an alpha particle and the energy of a conversion electron. These sum peaks would particularly be a nuisance in searching for alpha decay to the ground state of ^{206}Tl. The sum of the alpha particle energy for the alpha decay to the 266 keV excited state of ^{206}Tl and the L conversion

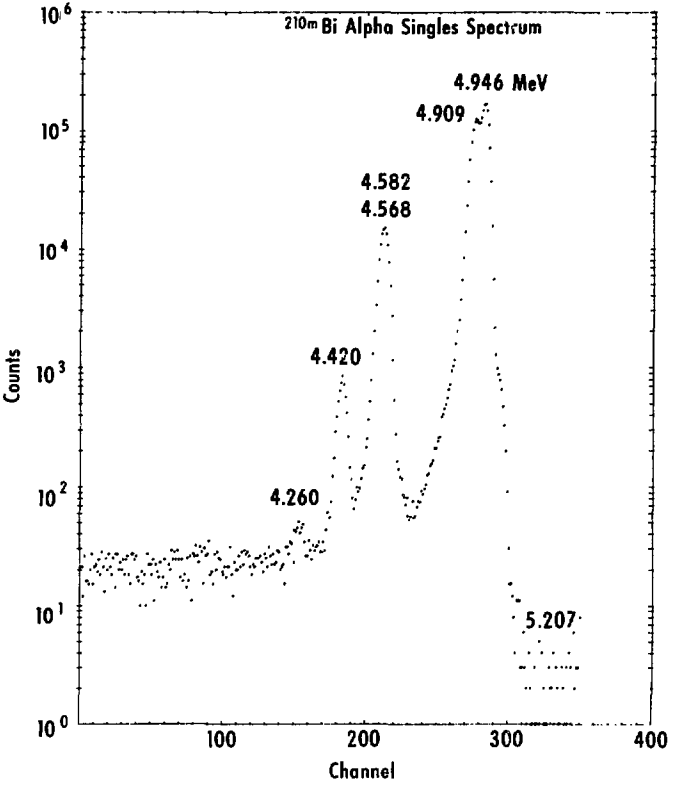

XBL7512-9958

electron energy for the internal conversion decay of the excited state, is only 10 keV less than alpha particle energy for the alpha decay to the ground state, and the resolution for the spectra was not high enough to separate two peaks that close in energy. A diagram of the counting chamber is shown in Fig. 9.

The ^{210m}Bi source and the detector were separated by a ¼" piece of metal with a ⅛" collimating hole cut in it. The metal piece was constructed of brass and steel so that when placed between the two poles of a large permanent magnet (firm contact must be made with both pole faces of the magnet) a strong magnetic field was created across the ⅛" hole.

Internal conversion electrons emitted from the source towards the detector were deflected by the magnetic field (~3000 Gauss) into the walls of the ⅛" hole and thus were prevented from reaching the detector. On the other hand the effect of the magnetic field on the path of alpha particles was negligible because of the very much lower charge to mass ratio of alpha particles as compared to electrons.

The energies and relative intensities of the peaks in the alpha spectrum of ^{210m}Bi were measured and are shown in Table 5 along with the results of references 6, 7, and 10.

The energies of the alpha peaks were determined by using the ^{210}Po peak at 5.305 MeV as a reference point and an energy scale derived from two ^{210m}Bi alpha peaks. Based on alpha-gamma and gamma-gamma coincidence data the assumption was made that the energy difference between the alpha decay leading to the 260 keV level of ^{206}Tl and the alpha decay leading to the 801 keV level of ^{206}Tl was 536 keV x $\frac{206}{210}$ = 526 keV. By using this value and the measured distance between these two alpha

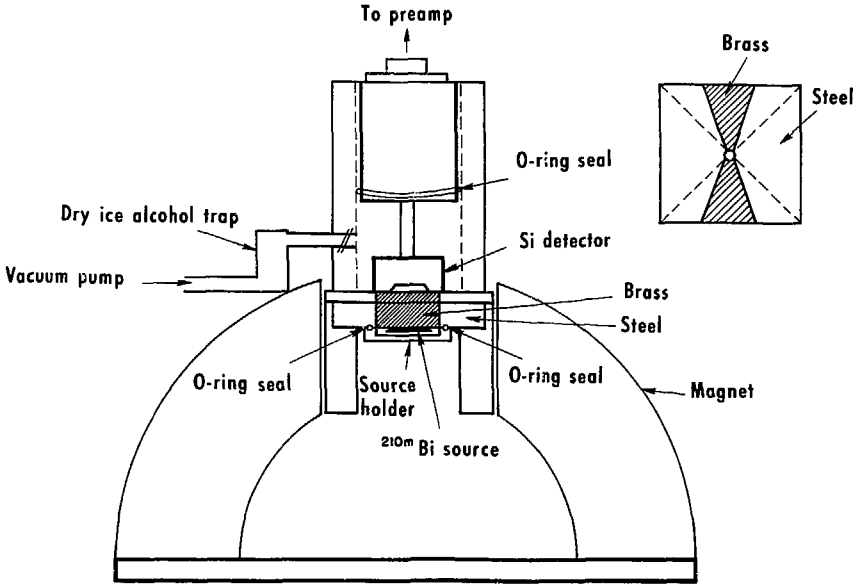

Figure 9. Alpha singles counting chamber.

Table 5. Alpha Energies and Branching Ratios for ^{210m}Bi

Present		Rusinov[7]		Korolev[10]		Lange[6]	
Energy[b]	Branching Ratio	Energy	Branching Ratio	Energy	Branching Ratio	Energy	Branching Ratio
5.207	$< 10^{-4}$					5.207	≈.04
4.946	55.0	4.936	60	4.959	57.6	4.935	54.6
4.909	39.5	4.896	34	4.922	36	4.896	40.4
4.582[a]	5.1	4.596	5	4.574	6	4.568	.95
4.568[a]						4.550	3.74
4.420	0.3	4.486	.5	4.431	.4	4.400	.19
4.260	.01	-	-	-	-	-	-

(a) Unresolved Doublet. Energies were obtained from alpha gamma coincidence data and have an accuracy of .002 MeV.

(b) Energies have an accuracy of .001 MeV.

peaks the energy scale of the spectrum was determined.

The intensities of the peaks in the alpha spectrum were measured by graphically drawing background curves and subtracting this background from the peak area. The alpha peak at 4.574 MeV is actually a sum of two peaks which could not be resolved in the alpha singles spectrum, so the intensity given in Table 5 is actually the sum of the intensities of both peaks. The energies and intensities of the two peaks were measured in the alpha-gamma coincidence spectrum and will be discussed in Section B5 of this chapter.

The alpha peak at 4.260 MeV had not been previously observed. It was identified as the alpha decay of ^{210m}Bi to a 952 keV excited state of ^{206}Tl based on the alpha decay energy and alpha-gamma coincidence data where a 4.268 MeV alpha peak was observed in coincidence with a 686 keV gamma ray. The 686 keV gamma ray was assumed to be produced by the decay of the 952 keV excited state of ^{206}Tl to the 266 keV excited state.

An alpha peak corresponding to the decay of ^{210m}Bi to the ground state of ^{206}Tl was not observed, but a lower limit was determined and is listed in Table 5. The importance of this lower limit is that it can be used to set a lower limit on the degree of parity mixing in either the isomeric state of ^{210}Bi or the ground state of ^{206}Tl.

The rules governing the spin and parity changes in alpha decay are relatively simple. If the spin of the parent nucleus if J_i and the spin of the daughter nucleus is J_F, then the emitted alpha particle can have an angular momentum relative to the daughter nucleus which falls between the following limits.

$$|J_i - J_F| < L < J_i + J_F$$

The parity change involved in the decay is governed by the value of L. If L is even then no parity change can occur. If L is odd, the parent and daughter nucleus must have opposite parities.

If $J_i \neq 0$ and $J_F \neq 0$ then the parity rules are not restrictive, but if either $J_i = 0$ or $J_F = 0$ or both $J_i = 0$ and $J_F = 0$, then the alpha decay can only occur with one value of L. For example, if $J_i = 9$ and $J_F = 0$, then the only allowed value of L is 9, and alpha decay is only allowed if the parent and daughter have opposite parity.

The spin of ^{210m}Bi is 9 and it has negative parity while the spin of the ground state of ^{206}Tl is 0[54] and it also has negative parity. As in the above example, decay of ^{210m}Bi to states with spin 0 is only allowed if they have positive parity.

Therefore alpha decay of ^{210m}Bi to ^{206}Tl will not occur unless a violation of the accepted rules concerning spin and parity occurs. One possible violation of the rules concerning parity would be the mixture of a slight amount of positive parity into the ground state of ^{206}Tl or into the metastable state of ^{210}Bi. A minimum value for the amount of

this abnormal parity mixing is calculated in Chapter III.

2. Gamma Singles

The gamma spectrum of ^{210m}Bi was studied with two different sources. One source was ~5 g of irradiated bismuth (0.13 atom % ^{210m}Bi) which had not been mass separated. This source contained ^{125}Sb and ^{207}Bi which were used as internal standards to determine the variation of detector efficiency with energy and to establish an energy scale for the spectrum. Energies and relative intensities of all but 4 gamma peaks in the ^{210m}Bi spectrum were measured using this source.

The second source was ~.35 mg of mass separated bismuth (~2% ^{210m}Bi). The mass separation removed the ^{125}Sb and greatly reduced the levels of ^{207}Bi and ^{208}Bi. This source was used to measure the energy and intensity of the ^{210m}Bi gamma peak at 635 keV which had been obscured by a gamma peak of ^{125}Sb, and to locate several very low intensity gamma peaks which were hidden by the background in spectra taken with the first source. Spectra taken with both of these sources will be discussed separately below.

The gamma spectrum of ^{210m}Bi was taken, using the 5 g source, with a 6 cm^2 Ge (Li) solid state detector. The absolute efficiency of the detector was measured as ~2.6% at 279 keV using a ^{203}Hg standard, and its resolution ranged from 1.6 keV at 266 keV to 2.3 keV at 1332 keV. A summary of the energies, peak areas, and relative intensities for the internal standards ^{125}Sb and ^{207}Bi is given in Table 6. The energies and relative intensities listed are from the literature whereas the peak areas listed were measured in this work. The measured energies and relative intensities of the peaks in the gamma spectrum of ^{210m}Bi are listed in Table 7 along with the results of References 9 and 6.

Table 6. Standards (^{125}Sb, ^{207}Bi)

	En[a]	Rel Int[a]	Peak area	
^{125}Sb	176.3	22.4	3.27×10^4	
	427.9	100	4.40×10^4	
	463.4	32.9	1.07×10^4	
	600.6	64.8	1.14×10^4	
	606.7	20.6	3.44×10^4	
	636.0	43.6	7.07×10^3	(Sum of ^{125}Sb, ^{210m}Bi)
^{207}Bi	569.7	100	1.57×10^6	
	1063.6	76	4.69×10^3	
	1770.2	7.5	2.08×10^4	

(a) Reference 28

Table 7. ^{210m}Bi Gamma Energies and Relative Intensities

Energy			Rel Int			
Present	Ref. 6	Ref. 9	Present	Ref. 6	Ref. 9	Peak Area (Present)
265.6	266	265.7	100	100	100	1.93×10^6
304.6	305	304.8	55.4	54	≈54	8.65×10^5
329.6	329	329.1	1.46	1.1	≈2	2.01×10^4
344.3	344	344.0	1.40	1.4	≈2	1.80×10^4
368.9	368	369.6	1.25	1.3	≈1	1.42×10^4
384[a]	-	-	.011[a]	-	-	
535.5	534	-	0.51	0.5	-	2.55×10^3
635[a]	634	-	.02	.02	-	-
649.6	651	649.8	7.7	5.6	≈4	2.32×10^4
686[a]	-	-	.012[a]	-	-	-
801[a]			>.005			

(a) Measured from a gamma spectrum taken with isotopically separated bismuth source (~2% ^{210m}Bi).

The values listed in Table 7 for the 384, 635, 686 and 801 keV peaks were measured using the isotope separated sample. The 384, 686, and 801 keV peaks were not seen in spectra taken using the unseparated bismuth source because their counting rates were too low in comparison to the Compton background counting rates caused by ^{207}Bi gammas. The 635 keV peak was obscured in the spectra taken using the unseparated bismuth by a gamma peak of ^{125}Sb at 636 keV.

Only a lower limit for the intensity of the 801 keV is listed because the measured intensity corresponds to that expected for a peak caused when two gammas (in this case a 536 and 266 keV) simultaneously strike the detector and create an electronic pulse which corresponds to the sum of their energies.

The 635 keV measured peak intensity also had a component caused by a sum peak. The intensity listed in Table 7 is the measured peak intensity minus the calculated intensity of the sum peak.

The peak areas were measured by using a computer code MAGIC developed by Janis Dairiki[25] and a CDC 6600 computer to fit a gaussian shape to the peak after subtracting background. An example of this peak fit is shown in Fig. 10 for the 1332 keV peak of ^{60}Co.

The gamma spectrum of ^{210m}Bi was taken using the mass separated sample with a 6 cm^3 intrinsic Ge detector. The efficiency of the detector was ~3.4% at 280 keV and its resolution was 1.5 keV at 330 keV.

The purpose for measuring the gamma spectrum of ^{210m}Bi with this source was to search for very low intensity gamma peaks which were hidden by the high background counting rates in the spectra taken with the unseparated sample. To keep the background counting rate from other sources in the room to a minimum, the detector and sample were enclosed

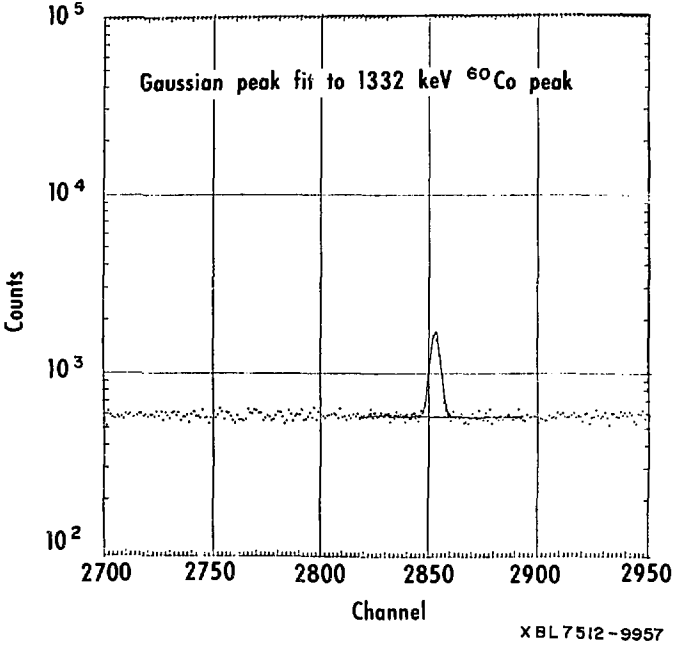

Figure 10. Gaussian peak fit to the 1332 keV ^{60}Co gamma peak.

in a lead cave. The spectrum recorded is shown in Fig. 11 and the energies and identification of the sources of the peaks are listed in Table 8. Two peaks that had not been previously observed were seen in this spectrum. They were at 384 keV and 686 keV. The 384 keV peak is produced by a gamma transition from the 650 keV excited state of ^{206}Tl to the 266 keV excited state. The 686 keV transition was identified as the decay of the 952 keV excited state of ^{206}Tl to the 266 keV level. This identification was supported by alpha gamma coincidence measurements where the 686 keV gamma appeared in coincidence with an alpha peak corresponding to the alpha decay of ^{210m}Bi to the 952 keV excited state of ^{206}Tl.

The intensities of the gamma peaks corresponding to gamma transitions in ^{206}Tl following a ^{210m}Bi alpha decay were calculated as before with the peak fitting program MAGIC.

For three of the gamma peaks (635, 650, and 801 keV) it was necessary to split the measured peak intensity into two components. One component was the intensity due to a single gamma ray with the appropriate energy. The second component was the intensity caused by two separate gammas with energies E_1 and E_2 such that $E_1 + E_2 = E_3$ where E_3 is the energy of the gamma peak being studied. If these two gammas strike the detector in coincidence they can give rise to a pulse corresponding to an energy E_3.

The 635 keV excited state of ^{206}Tl has three paths by which to decay to the ground state of ^{206}Tl. These are: 1) direct decay to the ground state, 2) decay to the 305 keV excited state of ^{206}Tl followed by the decay of the 305 keV excited state to the ground state, and 3) decay to the 266 keV excited state of ^{206}Tl followed by the decay of the 266 keV

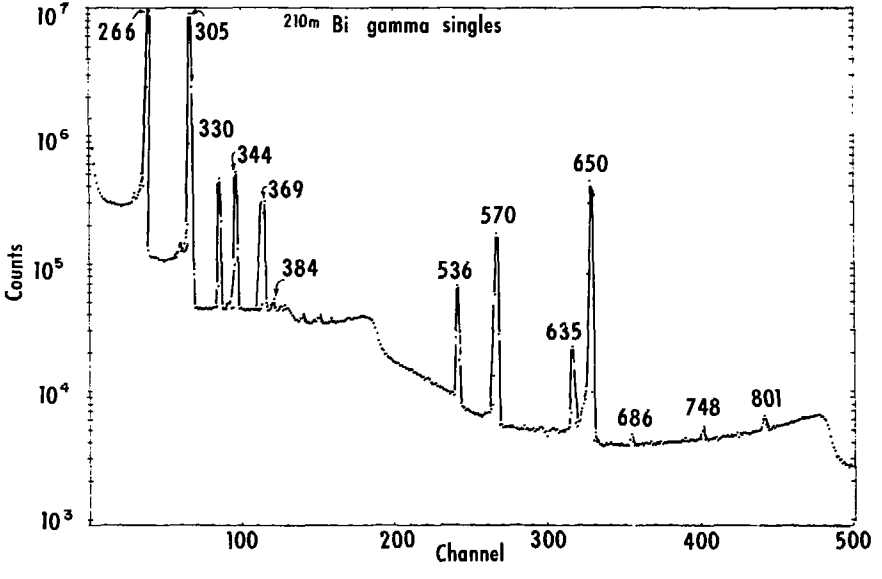

Figure 11. Gamma singles spectrum of ^{210m}Bi.

excited state to the ground state. All of the decays can occur by the emission of either a gamma ray or an internal conversion electron.

The measured intensity of the 635 keV peak was the sum of the intensities for these three paths where

$$I_M(635) = P_\alpha \left[\left(\frac{1}{1+\alpha_{635}} \right) \cdot E(635) \cdot R(635)_{635} + \left(\frac{1}{1+\alpha_{330}} \right)\left(\frac{1}{1+\alpha_{305}} \right) E(330)\, E(305)\, R(330)_{635}\, R(305)_{305} + \left(\frac{1}{1+\alpha_{369}} \right)\left(\frac{1}{1+\alpha_{266}} \right) E(266)\, E(369)\, R(369)_{635}\, R(266)_{266} \right]$$

and

$I_M(635)$ is the measured intensity of the 635 keV gamma peak in counts/min

P_α is the rate of ^{210m}Bi alpha decay to the 635 keV excited state of ^{206}Tl in d/min (feeding of the 635 keV excited state of ^{206}Tl from higher excited states is neglected)

α_ε is the conversion coefficients (K + L + M) listed in Table 12.

$\frac{1}{1+\alpha_\varepsilon}$ is the fraction of decays occuring by gamma emission

$E(\varepsilon)$ is the gamma detector absolute efficiencies for energy ε

$R_\varepsilon(\varepsilon')$ is the branching ratio for the excited state of ^{206}Tl with energy ε

ε' is the transition energy.

The 266 keV and 305 keV excited states of ^{206}Tl decay exclusively to the ground state and therefore

$$R(266)_{266} = R(305)_{305} = 1$$

The measured intensities of the 330 and 369 keV peaks can be expressed as

$$I_M(330) = P_\alpha\left(\frac{1}{1+\alpha_{330}}\right) R_{635}(330)$$

$$I_M(369) = P_\alpha\left(\frac{1}{1+\alpha_{369}}\right) R_{635}(369)$$

and substituting into the equation for the measured intensity of the 635 keV peak gives

$$I_M(635) = I_S(635) + I_M(330)\left(\frac{1}{1+\alpha_{305}}\right) E(305) + I_M(369)\left(\frac{1}{1+\alpha_{266}}\right) E(266)$$

where $I_S(635) = P_\alpha\left(\frac{1}{1+\alpha_{635}}\right) R_{635}(635)\ E(635)$

is the intensity in counts/min of the 635 keV gamma ray. Using this equation the value of I_S was calculated and used to calculate the relative intensity value shown in Tables 7 and 8 for the 635 keV gamma transition.

The relative intensities of the 650 and 801 keV gamma transitions were calculated following the same procedure as with the 635 keV gamma transition. For the 650 keV gamma transition $I_S(650) \simeq I_M(650)$ but for the 801 keV transition $I_S \ll I_M$. Therefore only an upper limit could be set for the relative intensity of the 801 keV gamma transition.

Table 8. ^{210m}Bi Gamma Singles Spectrum

Peak	Energy	Rel Int	Remarks
1	258		^{206}Tl 266 keVγ - 9 keV Ge X-ray escape
2	266	100	^{206}Tl transition (266 → 0)
3	296		^{206}Tl 305 keVγ - 9 keV Ge X-ray escape
4	305	56	^{206}Tl transition (305 → 0)
5	330	1.3	^{206}Tl transition (635 → 305)
6	338		^{206}Tl 266 keVγ + 71 keV Tl X-ray
7	340		^{206}Tl 266 keVγ + 73 keV Tl X-ray
8	344	1.4	^{206}Tl transition (650 → 350)
9	349		^{206}Tl 266 keVγ + 83 keV Tl X-ray
10	352		^{206}Tl 266 keVγ + 85 keV Tl X-ray
11	369	1.2	^{206}Tl transition (635 → 266)
12	376		^{206}Tl 305 keVγ + 71 keV Tl X-ray
13	378		^{206}Tl 305 keVγ + 73 keV Tl X-ray
14	384	.011	^{206}Tl transition (650 → 266)
15	388		^{206}Tl 305 keVγ + 83 keV Tl X-ray
16	390		^{206}Tl 305 keVγ + 85 keV Tl X-ray
17	401		^{206}Tl 330 keVγ + 71 keV Tl X-ray
18	403		^{206}Tl 330 keVγ + 73 keV Tl X-ray
19	416		^{206}Tl 345 keVγ + 83 keV Tl X-ray
20	419		^{206}Tl 345 keVγ + 85 keV Tl X-ray
21	536	.52	^{206}Tl transition (801 → 266)
22	570		^{207}Pb transition
23	635	.02	^{206}Tl transition (635 → 0)
24	643		^{207}Pb 570 keVγ + 73 keV Pb X-ray
25	645		^{207}Pb 570 keVγ + 75 keV Pb X-ray
26	650	7.5	^{206}Tl transition (650 → 0)
27	655		^{207}Pb 570 keVγ + 85 keV Pb X-ray
28	686	.012	^{206}Tl transition (951 → 266)
29	748		^{207}Pb 1771 keVγ double escape peak
30	801		^{206}Tl Sum event of 266 keVγ + 536 keVγ
31	834		Chance coincidence Sum of ^{207}Pb 570γ + ^{206}Tl 266γ
32	1063		^{207}Pb transition

Table 8. (cont.)

Peak	Energy	Rel Int	Remarks
33	1591		^{208}Pb 2615 keVγ double escape peak
34	1632		^{207}Pb Sum of 570 and 1063 keV γ's
35	1664		^{208}Pb 1591 keV double escape peak + 75 keV Pb X-ray
36	1769		^{207}Pb transition
37	2102		^{208}Pb 2615 keVγ single escape peak
38	2615		^{208}Pb transition
39	2670		^{208}Pb 2615 keVγ + 75 keV Pb X-ray

3. Gamma-Gamma Coincidences

The gamma-gamma coincidence spectrum of ^{210m}Bi was recorded using two Ge (Li) detectors. The detectors were placed with their axes at an angle of 90° and lead shielding was placed between the detectors to minimize the occurrence of false coincidences caused by the scattering of a gamma ray from one detector to the other. The source used for these measurements was the mass separated sample mentioned in the discussion of the gamma singles spectra.

The analyzer in this experiment was operated in a multi parameter mode. When the coincidence circuitry detected a coincidence, a gate was triggered and the electronic pulses due to the two gamma rays determined to be in coincidence were sent to the analyzer where each was converted to a channel number proportional to the energy of the gamma ray causing it. The channel numbers were then written in the next sequential analyzer memory word. When the analyzer memory became full its contents were automatically transferred to magnetic tape, it was cleared, and then began filling again with more data.

At the conclusion of the experiment the magnetic tapes were analyzed

using a 7600 computer and a code named MULTY written by Dave Gorman and modified for use in this particular experiment by the author.

The program reads the magnetic tapes and uses the data to construct either plots of one parameter in coincidence with some specified region of the other parameter or two dimensional scan maps. The plots look exactly like those produced by single parameter data and can be analyzed using the same techniques. An example of a scan map is shown in Fig. 12.

The scan maps are 40 x 40 arrays of a region specified by input instructions to the program. They are particularly useful in identifying false coincidences caused by the scattering of gamma rays out of one detector and into the other. The scattering events show up as a diagonal ridge whereas a true coincidence appears as a peak with two tails, one in the vertical and one in the horizontal direction. Examples of both a scattering ridge and a peak can be seen in Fig. 12.

Note that, because of space limitations in the computer output, the largest number that can be expressed on the scan may is 999. A number larger than 999, eg. 1123, is printed as +23. Then a second scan map is printed where all values have been divided by 100 so that 1123 appears as 11. This process of dividing by 100 is repeated again if necessary until all channels can be expressed as a three digit number.

Another advantage of the scan maps is that the background under a peak can be estimated fairly easily. If the peak occurs on a back-scattering ridge, then interpolation between points of the peak area can be used to estimate the background counting rate due to backscattered events.

Another source of background is caused by the Compton scattering of

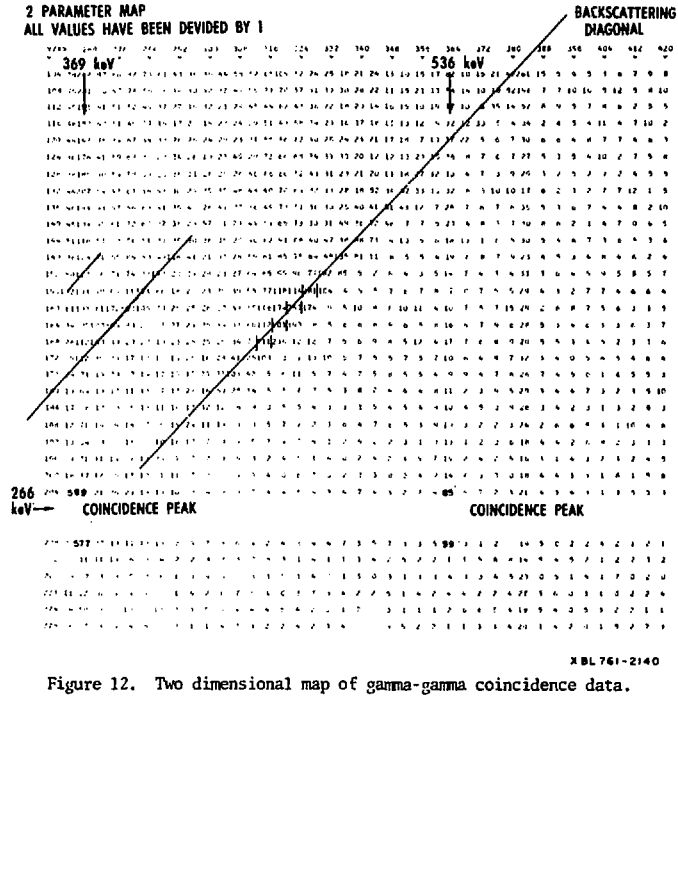

Figure 12. Two dimensional map of gamma-gamma coincidence data.

of one or both gammas involved in a true coincidence. This effect causes the horizontal and vertical ridges below each coincidence peak. At the point where two ridges, which originated from different coincidence peaks, cross a false peak occurs. This peak is due to the fact that the two sources of background are additive and the height of the false peak is simply the sum of the heights of the horizontal and vertical ridges.

Besides these horizontal and vertical ridges which are caused when only one gamma of a coincident pair is Compton scattered, background is produced over a large area by the Compton scattering of both gammas of a coincident pair. This background caused by Compton scattering of both gammas is reasonably smooth and its value under a coincidence peak can be estimated from channels below and to the right of the coincident peak.

One other source of background is the chance coincidence which can occur between two unrelated gammas. This background rate was measured by adjusting the timing on the coincidence circuitry so that the pulses from one detector were delayed by several μsec. This delay caused all real coincidences to appear as if they occurred several μsec apart and were not in coincidence. But the chance counting rate is not affected by this timing change, and was recorded and found to be negligible in comparison with other background sources.

Analysis of the gamma-gamma coincidence data for ^{210m}Bi showed the same four coincidence peaks seen by reference 6. They are listed in Table 9. The measured intensities of these peaks can be used to confirm the gamma ray intensities measured by gamma singles. The ratio between the 369 keV and 536 keV gammas in coincidence with the 266 keV γ should be

the same as the ratio measured in gamma singles. Likewise the ratio between the 330 keV γand the 345 keV γ in coincidence with the 305 keV γ should be the same. A comparison of ratios measured from gamma singles and measured from gamma-gamma coincidence data is shown in Table 9.

Table 9. Gamma-Gamma Coincidence Peaks

	γ_1	γ_2	Coinc Ratio	γ_2 Singles Ratio
1	266	369	2.53	2.50
2	266	536		
3	305	330	1.03	1.04
4	305	345		

4. Conversion Electron Singles

The internal conversion electron spectrum of ^{210m}Bi was recorded using a 0.785 cm^2 x 5 mm active area Si (Li) gold surface barrier detector. Using a ^{249}Cf source the resolution of this detector was measured as 2.2 keV at an electron energy of 262 keV. The efficiency of the detector was measured in terms of electrons/(100 ^{249}Cf alphas) where both the electron and alpha counting rates were measured with the same detector.

Since the geometric efficiency of the detector is the same for both alphas and electrons, the ratio of their counting rates needs only to be multiplied by an intrinsic efficiency factor which is the ratio of the instrinsic efficiencies of the detector for electrons and alpha particles. The instrinsic efficiency of the detector for electrons is less than that for alpha particles because electrons striking the detector

can be scattered backwards out of detector with a much higher probability than the much heavier and more energetic alpha particles.

Using the data of reference 26 and the measured conversion electron/(100 ^{249}Cf alphas) ratios for several conversion electron peaks in the ^{249}Cf conversion electron spectrum, the plot of the instrinsic efficiency ratio shown in Fig. 13 was constructed. This plot was used to obtain factors to multiply conversion electron/alpha counting ratios for ^{210m}Bi by so that conversion coefficients could be determined for the transitions between levels of ^{206}Tl.

The ^{210m}Bi source used to record the conversion electron spectrum was the collector foil from the isotope separation conducted at Lawrence Berkeley Laboratory.

The conversion electron spectrum of ^{210m}Bi is shown in Fig. 14. The resolution of the 180 keV peak was 2.1 keV. The various peaks in the spectrum were identified and their peak areas minus background were calculated. In Table 10 the intensities for the various transitions are shown where all intensities have been normalized to the intensity of the 180 keV transition (266 K conversion). The method by which the conversion coefficients were calculated will be briefly discussed below.

The K conversion coefficient for the 266 keV transition of ^{206}Tl was the only conversion coefficient which was calculated directly from the electron/alpha counting ratio. The other conversion coefficients were calculated using only the relative intensities of the gammas measured from the gamma singles spectrum and the relative intensities of the conversion electrons where both sets of relative intensities (gamma and conversion electron) were normalized to the 266 keV transition of ^{206}Tl.

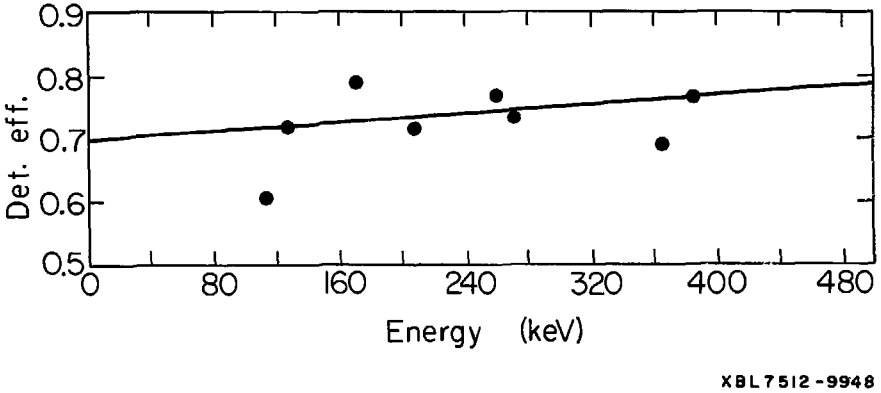

Figure 13. Electron detector efficiency.

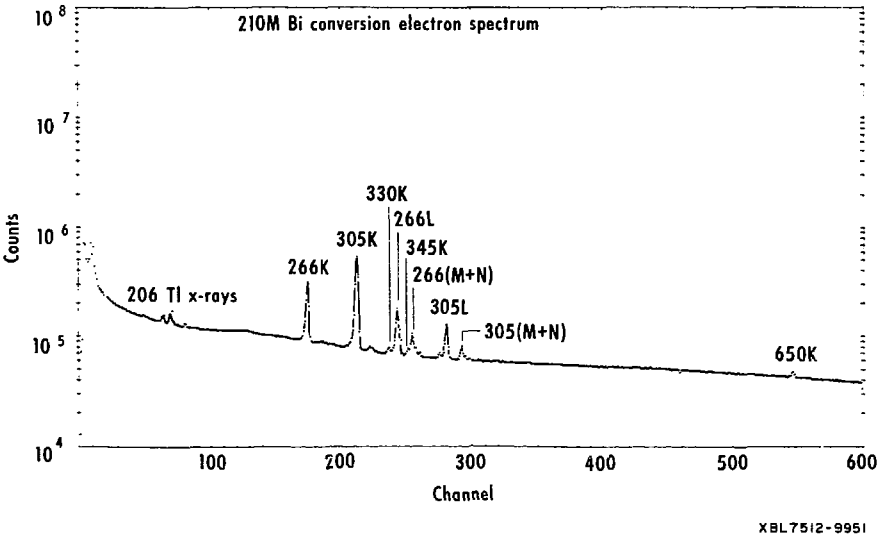

Figure 14. Conversion electron spectrum of ^{210m}Bi.

Table 10. Conversion Electron Intensities

Transition	Counting Rate/1000 min	Det Eff	Rate/ Eff	Rel Int
266K	6208	.73	8504	100
266L	3853	.74	5207	61
266M	867	.74	1170	14
305K	14,077	.74	19,000	220
305L	2304	.75	3070	36
305M	651	.75	868	10
330K	298	.74	403	4.7
	77	.75	100	1.2
345K	144	.74	195	2.3
	33	.76	43	0.51
369K	156	.75	210	2.5
369L	36	.76	47	.55
650K	162	.81	200	2.4

The equation used to calculate the conversion coefficients was

$$\alpha_{X,E} = \alpha_{K,266} \times \frac{I_{X,E}}{I_{Y,E}}$$

where

$\alpha_{X,E}$ is the conversion coefficient to be calculated

X refers to the shell from which the conversion electron is ejected

E refers to the transition energy

$\alpha_{K,266}$ is the K conversion coefficient for the 266 keV transition

$I_{X,E}$ is the relative intensity of the conversion electron peak for the transition of interest

$I_{\gamma,E}$ is the relative intensity of the gamma peak for this transition

The K conversion coefficient for the 266 keV transition was calculated from the ratio of 266 K conversion electrons to alphas leading to the 266 keV excited state of ^{206}Tl. This ratio was measured in the same manner as discussed earlier for ^{249}Cf. The measured conversion electron counting ratio was corrected for detector efficiency by using Fig. 13.

The number of alpha decays leading to the 266 keV excited state is a sum of three terms. The largest is due to alpha decay directly to the 266 keV excited state. The second is due to alpha decay to the 635 keV excited state followed by a transition from this excited state to the 266 keV excited state. The third term is similar to the second, but is for the 801 keV excited state.

Alpha branching ratios used in the calculation were obtained from alpha-gamma coincidence measurements. These branching ratios were calculated using theoretical electron conversion coefficients. Then after the conversion coefficients were calculated, these alpha branching ratios were recalculated and then the conversion coefficients were recalculated.

The branching ratio for decay of the 635 keV excited state to the 266 keV excited state of ^{206}Tl was also calcuated from alpha-gamma coincidence data using theoretical values for the conversion coefficients. The 801 keV excited state was assumed to decay only to the 266 keV

excited state. The parameters discussed above are shown in Table 11.

Table 11. Parameters Used to Calculate α_K (266 keV)

Alpha Branching Ratio	4.946	.56
	4.589	.016
	4.417	.0023
Branching Ratios for 635 keV excited state decay		
	635 → g.s.	.08
	635 → 266	.46
	635 → 305	.46

Total Branching Ratio for decays leading to 266 keV excited state = .57

Total alpha (^{210m}Bi) Decay Rate = 187,490 counts/1000 min
Alphas leading to 266 keV excited state = 107,000/1000 min

Electron Counting Rate	6208/1000 min
Electron Efficiency	0.73
Electron Counting Rate/Eff	8504/1000 min
266K conversion electrons/100 alphas[(a)]	7.95

(a) Only alphas leading to the 266 keV excited state of ^{206}Tl

The number of 266 keV gammas per 100 alphas leading to the 266 keV excited state of ^{206}Tl was calculated as follows:

$$N_\gamma = 100 - N_K - N_L - N_M$$
$$= 100 - 7.95 - 4.85 - 1.11 = 86.1$$

where

N_γ is the number of γs/100 alphas

N_i is the number of conversion electrons per 100 alphas for the K, L, and M electron shells

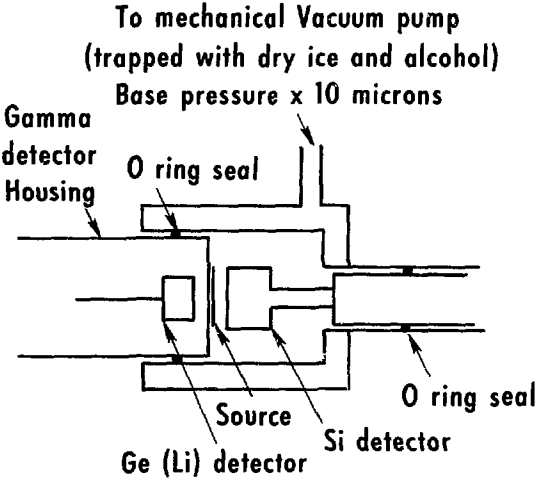

Figure 15. Diagram of detector and source locations for alpha gamma coincidence measurements.

And finally the conversion coefficient was calculated

$$\alpha_{K266} = \frac{N_K}{N_\gamma} = \frac{7.95}{86.1} = .092$$

Using this value and the equation discussed earlier, the internal conversion coefficients were calculated and are listed in Table 12 along with some values for the conversion coefficients calculated[27] using the multipolarities listed in the Table.

Table 12. Conversion Coefficients for ^{206}Tl
Calculated using $\alpha_K(266) = .092$

Transition (Multipolarity)	Electron Intensities	Gamma Intensity	Ratio Electron/ Gamma	Conversion Coefficient (Th[a])		K Line Norm to 1
266K (E2)	100	100	1	.092	(.086)	
266L	61	100	.61	.057	(.058)	.61
266M	14	100	.14	.013		.14
305K (M1)	220	55	4.0	.37	(.32)	1
305L	36	55	.65	.060	(.05)	.16
305M	10	55	.18	.017		.016
330K (M1)	4.7	1.5	3.1	.29	(.26)	1
330L	1.2	1.5	0.8	.074	(.04)	.26
345K (M1)	2.3	1.4	1.6	.15	(.23)	1
345L	0.5	1.4	.36	.033	(.04)	.22
369K (M1)	2.5	1.3	1.9	.18	(.19)	1
369L	.53	1.3	.41	.038	(.03)	.20
635K	< .5	.02	-	-	(.013)	
650K (M1)	2.4	7.7	.31	.029	(.047)	1

(a) Theoretical values for the indicated multipolarities taken from reference 27.

5. Alpha-Gamma Coincidences

The alpha-gamma coincidence spectrum of ^{210m}Bi was recorded using a 6 cm^3 Ge(Li) gamma detector and a 150 mm^2 active area gold surface barrier silicon alpha detector and the ^{210m}Bi source produced by the isotope separator.

The detectors and ^{210m}Bi source were arranged as shown in Fig. 15. The efficiency of the Ge(Li) detector was calibrated using standard sources of ^{241}Am, ^{22}Na, ^{137}Cs, ^{57}Co, ^{54}Mn, and ^{60}Co. This calibration was checked by recording a ^{210m}Bi gamma singles spectrum and comparing the relative intensities calculated using this efficiency calibration to the relative intensities discussed in Section B2 which were calculated using ^{125}Sb as an internal standard.

The absolute efficiency of the detector at 266 keV was 2.85% and at 650 keV, .46%.

The resolution of the Si detector was measured using the ^{210m}Bi source as 25 keV at 4.420 MeV.

The alpha-gamma coincidence data was recorded in the same multi-parameter mode discussed in Section B3 for gamma-gamma coincidence data.

Two sets of alpha-gamma coincidence data were collected. The first set of data had a lower energy cutoff at a gamma energy of 85 keV so that coincident events involving gammas with an energy less than 85 keV (primarily X-rays) would not be recorded. The purpose of making this energy cutoff was to reduce the overall volume of data recorded on magnetic tape. The second data set had a lower gamma energy cutoff of 450 keV. Again the purpose of this energy cutoff was to limit the overall volume of data recorded while increasing the amount of data collected for gammas with energies greater than 450 keV by running for a longer

period of time.

A diagram of the equipment used to record the first data set is shown in Fig. 16. Pulses from the gamma detector were fed to two linear amplifiers. Two different amplifiers were used so that the signal going to the coincidence circuitry could be amplified more than the signals going to the analyzer. The single channel analyzer was set to gate only on gammas above 85 keV to produce the energy cutoff discussed earlier.

Pulses from the alpha detector were fed to the linear amplifiers. A pulser signal corresponding to an energy of 5.500 MeV was fed into the pre-amplifier and was used by the analyzer for gain stabilization.

A second output from linear amplifier #2 is shown going through an energy window to the ADC. The energy window was set so that only pulses corresponding to an alpha energy range of ~5.3-5.7 MeV would trigger it. The signal from this energy window was then sent as a gate pulse to the ADC. These gate pulses identified those alpha pulses which were to be used for stabilization but not recorded.

The box labeled COINC contains circuits which determined when an input signal from the gamma side was in coincidence (±1 μs) with a pulse from the alpha side. When it recognized a coincidence it sent a gate pulse to both ADC's which told them to store the pulses they were processing (gate pulses arrived ~2μs after the signal pulses). The purpose of the delay is simply to delay the signal pulses to prevent them from reaching the ADC's before the coincidence gate. A summary of the data collected in this run is shown in Table 13.

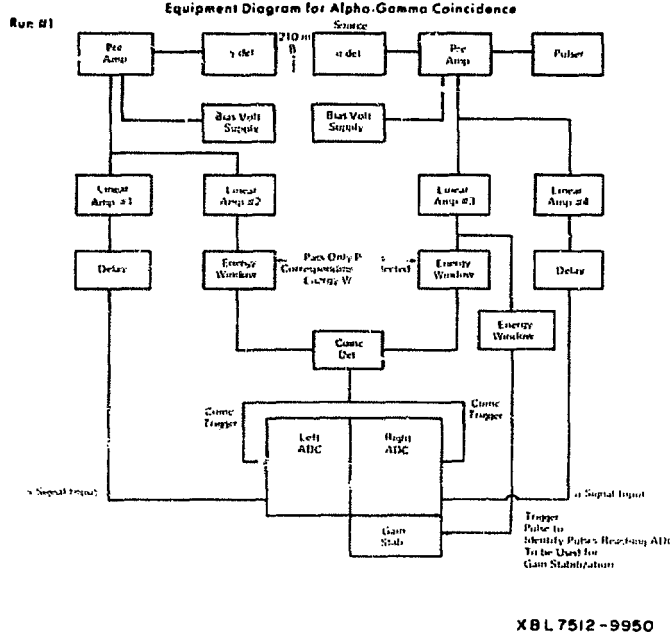

Figure 16. Equipment schematic for alpha-gamma coincidence run #1.

Table 13. Alpha Gamma Coincidence Data Run #1

	Alpha Energy	Gamma Energy	Counts (Corrected for Det Eff. & Conv. Coef.)	Rel Int	Alpha Branching Ratio		
					α γ (c)		α singles
1	4.420	266	1812	.37	.21		.3
2	4.420	536	(a) 1944	.39			
3	4.582	266	6746	1.4			
4	4.582	305	(b) —				
5	4.582	330	6537	1.3	1.4		
6	4.582	369	5891	1.2			
7	4.582	635	(a) 348	.07		5.3	5.1
8	4.568	305	(b) —				
9	4.568	345	6240	1.3	3.9		
10	4.568	650	28550	5.85			
11	4.909	305	341000	69.9	38.8		39.5
12	4.946	266	488000	100	55.5		55.5

(a) Use theoretical Values for the conversion coefficient

(b) Unresolved doublet of the 4.582 and 4.568 MeV alphas in coincidence with the 305 keV gamma

(c) Abundances from coincidence measurements normalized to 100%.

The alpha energies of the coincidence peaks were calculated by using as reference points the two ^{210m}Bi alpha peaks whose energies had been measured as 4.946 and 4.420 MeV in alpha singles spectra. The accuracy of the energies listed in Table 13 is ± 2 keV. The energies of the two alpha peaks which could not be resolved in the alpha singles measurements were found to be 4.584 and 4.568 MeV.

The gamma energies of the coincidence peaks were calculated by using an energy scale calibrated with the standards ^{60}Co, ^{22}Na, ^{54}Mn, ^{137}Cs, and ^{57}Co, and are accurate to ± 1.0 keV.

The relative intensities of the coincidence peaks were calculated by multiplying the measured peak area by the factor

$$\frac{(1 + \alpha_T)}{\text{Eff.}}$$

where α_T is the sum of the K, L, and M conversion coefficients

and Eff is the relative detector efficiency for the gamma ray involved in the coincidence

The alpha branching ratios were calculated by summing the relative intensities for all of the coincidences involving an alpha with a particular energy. The only exception to this was that all of the coincidences involving the 266 and 305 keV gammas were not included in the sums except for the 4.946 and 4.909 MeV alphas. These relative intensity sums were normalized so that their total equaled 100 and are listed in Table 13.

A diagram of the equipment used to record the second alpha-gamma coincidence data set is shown in Fig. 17. The equipment on the gamma side was the same as for the first data set except that the energy cutoff of the single channel analyzer was raised to 450 keV.

Several changes were made on the alpha side. The pulser was removed and gain stabilization was accomplished using the 4.909-4.946 MeV doublet of ^{210m}Bi. The single channel analyzer (2) was set so that it would give output pulses only for input pulses corresponding to an alpha particle with an energy greater than 4.7 MeV.

Equipment Diagram For Alpha-Gamma Coincidence Run #2

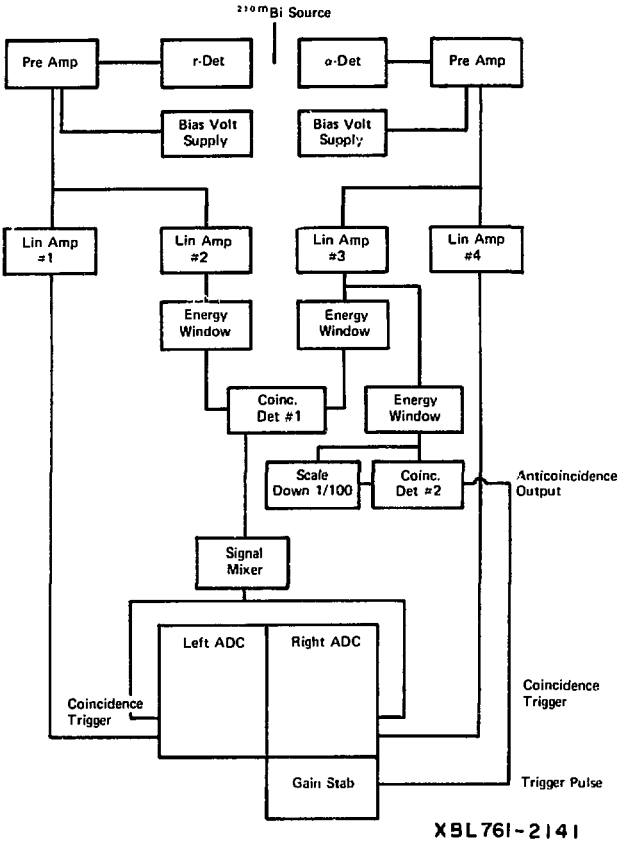

Figure 17. Equipment schematic for alpha-gamma coincidence run #2.

The output pulses from single channel analyzer (2) were split into two groups by the scale down unit and coincidence unit (2). Ninety-nine out of a hundred pulses were sent to the gain stabilization trigger. The pulses triggered the gain stabilization unit to look at the alpha pulse in the ADC and use it for gain stabilization.

One out of every one hundred pulses out of the single channel analyzer (2) was sent through the linear gate to the ADC's as a coincidence signal, indicating that the pulses being processed in the ADC should be stored. Thus one out of every one hundred alphas with energy greater than 4.7 MeV was stored as a coincidence event regardless of whether it actually occurred in coincidence with any gamma. (If no gamma pulse is in the ADC when it receives a coincidence trigger, the event is stored as the coincidence of an alpha with a gamma in channel zero.)

The purpose of recording 1% of the singles alpha pulses with energy greater than 4.7 MeV was to produce a peak in the data which could be used as an energy reference point.

A summary of the data recorded in this second alpha-gamma coincidence run is shown in Table 14. Three alphas were observed in this run which had not been seen in the first run because of their low intensities.

The alpha and gamma energies of the coincidence peak were calculated in the same manner as with the first alpha gamma coincidence run. The accuracy of the alpha energies decreased to ± 8 keV because of gain changes in the electronics.

Three of the coincidences observed in this run were also seen in the first alpha gamma coincidence run. These are the last three coincidences listed in Table 14.

Table 14. Alpha-Gamma Coincidence Data Run #2

	Alpha[a]	Coinc Peak Energy ^{206}Tl level[c]	Gamma[b]	Relative Intensity
1	4.100	(1126)	457	1 x 10^4
2	4.100	(1126)	536	2 x 10^4
3	4.100	(1126)	650	1.2 x 10^5
4	4.100	(1126)	1120	7 x 10^4
5	4.230	(996)	734	8 x 10^4
6	4.268	(952)	687	6 x 10^3
7	4.417	(801)	536	.29
8	4.574	(650)	650	6.5
9	4.589	(635)	636	.17[d]

[a] Accuracy is ± 8 keV

[b] Accuracy is ± 2 keV

[c] Calculated by subtracting the alpha particle energy and ^{206}Tl recoil energy from the Q value for the alpha decay of ^{210m}Bi to the ground state of ^{206}Tl.

[d] This intensity is primarily due to sum peaks and not a single 635 keV gamma.

III. Calculations of Alpha Decay Rates

A. Introduction

As early as 1912 Geiger and Nuttal[29], based on a systematic study of alpha decay half lives and alpha particle ranges, were able to show that the logarithm of the decay constant varied linearly with the logarithm of the alpha particle range. With this relationship the first calculations of alpha decay constants were done and indeed, the half life of Ionium (^{230}Th) was successfully predicted before it had been measured experimentally.

A model for alpha decay which successfully explained this empirically derived relationship between alpha decay half lives and energies was developed independently by Gamow[30] and by Condon and Gurney[31] in 1928. This model assumes that an alpha particle exists inside the nucleus and that it interacts with the other nucleons through an attractive square well potential which is bounded at the nuclear surface. Outside of the nucleus a repulsive Coulomb potential is used to describe the interaction between the alpha particle and the remaining nucleons inside the nuclear volume.

In a classical treatment of this model the escape of the alpha particle from the square well is not possible unless it has a total energy greater than the height of the Coulomb barrier, but in the quantum mechanical treatment used by Gamow and by Condon and Gurney, an alpha particle with a total energy greater than zero has a finite probability of tunneling through the Coulomb barrier. The probability of alpha decay (i.e., escape of the alpha particle from the square well) is the product of two terms. The first is a measure of the number of times that the alpha hits the barrier in some unit time (usually one second). The second factor is the probability that an alpha particle that hits the barrier will tunnel through it instead of bouncing back into the square well. Both factors are functions of the alpha decay energy but the frequency factor only varies by a factor of 1.5 over a range of alpha decay energies 4 to 8 MeV, while the barrier penetration factor changes by more than thirteen orders of magnitude over this same energy range and also reproduces the energy half life relationship observed by Geiger and Nuttal[29].

Calculations of alpha decay rates using this model were relatively successful for predicting the ground state to ground state alpha transitions in even-even nuclei, but calculations for odd-odd nuclei and for

transitions to excited states in even-even nuclei consistently gave values that were higher than experimental values. This led to the use of hindrance factors to represent the ratio between experimental alpha decay rates and calculated alpha decay rates.

The necessity of using hindrance factors indicated that although this simple model accurately described the energy dependence of alpha decay rates through the barrier penetration factor, a more sophisticated treatment of the behavior of the alpha particle inside the nucleus was needed. Indeed the existence of a reformed alpha particle moving freely around inside the nucleus at all times did seem rather improbable, and attempts were made to redefine the alpha particle nucleus potential.

Winslow[32] modified the square well potential by localizing it at the nuclear surface. This model assumed the existence of a preformed alpha particle on the nuclear surface only, instead of throughout the whole nuclear volume.

Calculations of alpha decay rates using this model were still too large, but Winslow offered a possible explanation. He proposed that alpha particles do not exist in the surface well at all times but are constantly being formed at the nuclear surface with some finite probability. Once formed the alpha particle can either tunnel through the Coulomb barrier and escape from the nucleus or break up into four nucleons.

Winslow suggested that the alpha decay constant should be expressed as a product of the probability of an alpha particle existing in the surface well and the probability that an alpha particle in the surface well will escape through the Coulomb barrier, but he did not develop a method for calculating the probability for an alpha particle to form at the nuclear surface.

The development of a formalism for calculating alpha particle formation probabilities at the nuclear surface was accomplished by Hans Mang[2-5]. In this formalism which is outlined in the next section, the formation probability for an alpha particle at the nuclear surface is calculated using nuclear model wave functions. This formation factor is then multiplied by a barrier penetration term to give the alpha decay constant.

Using this formalism Mang[2-5] was able to obtain agreement with experimental results except for some problems with absolute values. The usefulness of Mang's model was also demonstrated by Poggenburg[33] and by Mang and Rasmussen[34].

Because of this success of Mang's formalism for calculating relative alpha decay rates it was chosen for use in calculating alpha decay rates for ^{210}Bi. In the next section a brief summary of Mang's equations will be presented. Following that a brief description of the method of calculation used in this work, and the results of alpha decay calculations for ^{211}Po, ^{211m}Po, ^{210m}Bi, and ^{210}Bi will be presented.

B. Review of Mang's Equations

The alpha decay constant for a nucleus with A nucleons can be calculated easily if the time dependent wave function Φ (1...A,t) for the system can be determined, but at present the determination of the wave function for all but very simple nuclei is impossible. Instead nuclear properties such as alpha decay constants are calculated using approximate nuclear wave functions.

For calculating alpha decay constants two sets of time independent approximate wave functions are combined to get an appropriate time dependent wave function. This combination of two sets of time independent

wave functions is necessary because one set, nuclear model wave functions*, is a good approximation only if all of the nucleons are contained inside some nuclear radius R and the other set is valid only for a nucleus with A-4 nucleons and an alpha particle separated by a distance larger than R_o. The definitions of R and R_o are shown in Fig. 17a.

Mang's expression for the time dependent wave function shown below was derived from an expression used by Casimir[35].

$$\Phi(1\ldots A,t) = a(t)\,\Phi_{\alpha J}^{M}(1\ldots A) + \sum_{J\sigma L}\int d\varepsilon\; b_{J\sigma L}(\varepsilon,t)\,\mathcal{A}\,\{\chi_\alpha \Phi_L(R,\varepsilon)\sum_m C(Lj\,J;\,m\;M\text{-}m)\,Y_L^m(R/R)\,\Psi_{j\sigma}^{M-m}(1\ldots(A-4)\}$$

where

$\Phi_{\alpha J}^{M}(1\ldots A)$ and $\Psi_{j\sigma}^{M-m}(1\ldots(A-4))$

are nuclear model wave functions with angular momentum J and j.

σ is used to represent all other quantum numbers for the wave function Ψ.

χ_α is a wave function for the internal degrees of freedom of an alpha particle

$\mathcal{A}$ is an antisymmeterization factor

C (LjJ;m M-m) is a Clebsch-Gordon coefficient

$\Phi_L(R,\varepsilon)$ is a radial wave function for the reduced center of mass

---

*Shell Model wave functions were used in this work.

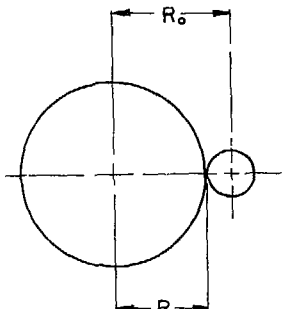

Figure 17a. Relationships between R and R_o.

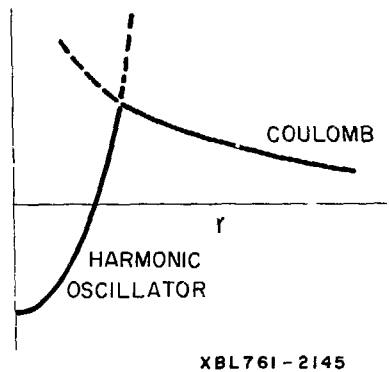

Figure 17b. Harmonic oscillator and coulomb potentials.

of an alpha particle in the Coulomb* field produced by a nucleus with Z protons

Y_L^m (R/R) is the angular part of the wave function for the center of mass of an alpha particle in the Coulomb field produced by a nucleus with Z protons

ϵ is the total energy for the alpha reduced center of mass interaction with the nucleus

a(t) and $b_{J\sigma L}(\epsilon,t)$ are the coefficients which link the two time independent approximate solutions to give a time dependent solution

The first term of Mang's approximate time dependent wave function is a nuclear model wave function for a nucleus with A nucleons. A typical shell model harmonic oscillator potential is shown in Fig. 17b. The second term is an approximation to the wave function for a system consisting of a nucleus with A-4 nucleons and an alpha particle where the only interaction between the alpha particle and the nucleus is via the Coulomb* potential which is shown in Fig. 17b.

The reason for using a combination of two approximate wave functions is that the actual potential between an alpha particle and a nucleus with A-4 nucleons can best be approximated by using some nuclear model potential out to a radius R_o and outside of this radius using the Coulomb potential. For this potential shown in Fig. 17b the appropriate wave function is that used by Mang.

An expression for the alpha decay constant can be obtained by using Mang's wave function in a Schrodinger equation and using various approximation techniques.[3] The expression derived is

*Other potentials can be used for the interaction of a nucleus with A-4 nucleons with an alpha particle. The effect will only be seen in $\Phi_{l_i}(R,\epsilon)$.

$$\lambda = \frac{2\pi}{\hbar} \sum_L \left| \frac{\hbar^2}{2M^1} \; R_o^{\frac{1}{2}} \; \Phi_L(R_o) \left(\frac{\delta G_{jL}^{J}(R_o)}{\delta R_o} - G_{jL}^{J}(R_o) \; \frac{\delta \Phi_L(R_o)/\delta R_o}{\Phi_L(R_o)} \right) \right|^2$$

where

$$G_{jL}^{J}(R_o) = R_o^{\frac{3}{2}} \int d\,\xi_K \; d\,\xi_\alpha \; d\,\Omega_{Rel}$$

$$\left[\Phi_{\alpha J}^{M} \; \chi_\alpha(\xi_\alpha) \sum_m C(L_J J_i \; m \; M-m) \; Y_L^m(\Omega_{Rel}) \; \Psi_{J\sigma}^{M-m}(\xi_K) \right]$$

$$\Phi_L(R_o) = \left(\frac{2M}{\pi\hbar^2} \right)^{\frac{1}{2}} \frac{1}{2R_o \; q_L^{\frac{1}{2}}(R_o)} \exp\left(- \int_R^{R_\mu} q_L(R)\, dR \right)$$

$$q_L(R) = \left\{ \frac{2M}{\hbar^2} \left[\frac{2(Z-2)e^2}{R} - \frac{\hbar^2}{2M} \frac{L(L+1)}{R^2} - \epsilon \right] \right\}^{\frac{1}{2}}$$

R_μ is the outer turning radius such that $q_L(R_\mu) = 0$

M is the reduced mass of the alpha particle

A simplified form of this equation derived by Mang[2] is shown below.

$$\lambda = \frac{1}{\hbar} \sum_L P_L(\epsilon) \; \gamma_{JjL}^2$$

$$P_L(\epsilon) = 2R_o \; q_L(R_o) \exp\left(-2 \int_{R_o}^{R_\mu} q_L(r)\, dr \right.$$

$$\gamma_{JjL}^2 = \frac{\hbar^2}{2MR_o^2} \; |G_{jL}^{J}(R_o)|^2$$

A computer code was developed to calculate alpha decay probabilities using this expression. A discussion of the procedures and steps of the calculation is given in the next section.

C. Calculation Description

The calculation of alpha decay constants using Mang's equation involves the calculation of two terms. The first, the penetrability factor, involves a fairly straightforward integration which can be done analytically if the Coulomb potential is used. Calculation of the second term, though, the reduced width, is fairly complicated and involves calculating the value

$$G_{jL}^{J}(R_o) = R_o^{\frac{3}{2}} \int \sum_{m} C(LjJ;m\ M\text{-}m)$$

$$X_\alpha(\xi_\alpha)\ Y_L^m(\Omega_{Arel})\ \psi_j^{M-m}(\xi_K)\ \Phi_{oJ}^{M}\ d\xi_K\ d\xi_\alpha\ d\Omega_{rel}$$

where

ξ_α are the internal coordinates for the alpha particle

ξ_K are the internal coordinates for the daughter nucleus

Ω_{rel} are the angular coordinates for the alpha particle relative to the daughter nucleus

To calculate this integral the first step that must be taken is to separate the shell model wave function Φ_{oJ}^{M} into two parts; one, a core wave function with angular momentum quantum numbers equal to those of the daughter nucleus; and the second, a wave function for four particles* coupled to a total angular momentum L.

$$\Phi_{oJ}^{M}(1\ldots A) = \sum_{mo} C_o\ C(LjJ;\ m\ M\text{-}m)$$

$$\phi_{Kj}^{M-m}(1\ldots(A-4))\ \Phi_{AL}^{m}(1',2',3',4')$$

---

*Two protons and two neutrons

where

σ represents various intermediate quantum numbers such as the total proton or neutron angular momentum which must be summed over

C_σ is a product of all the coefficients produced in factoring the wave function. It is a function of the quantum numbers of the single particle wave functions making up Φ_{AL}^{m} (1,2,3,4), the total proton angular momentum of the two protons in the four particle wave function, the total neutron angular momentum of the two neutrons in the four particle wave function, and other possible intermediate angular momenta.

1,2,...(A-4) refer to the radial and angular coordinates of the nucleons not in the four particle wave function

1',2',3',4' refer to the radial and angular coordinates of the nucleons in the four particle wave function

The exact method used to split $\Phi_{\sigma J}^{m}$ (1...A) into two factors is dependent on the nucleus involved. Detailed descriptions of the method used for the nuclei discussed in this work can be found in Appendices A and B.

The next step in the calculation is to assume that the shell model wave functions ψ_J^{M-m} and $\Phi_{\sigma J}^{m}$ (and consequently Φ_{KJ}^{M-m}) are based on the same harmonic oscillator potential parameters so that

$$\int \psi_J^{M-m} \Phi_{KJ}^{M-m} \, d\xi_K = 1$$

where ξ_K represents the radial and angular coordinates of all of the nucleons (1...(A-4)).

Also, the use of the magnetic quantum number and Clebsh Gordon coefficients is dropped. The value of the integral is independent of m so that the Clebsch Gordon coefficient if carried through appears in the final result as

$$\sum_{m} D \cdot \left[C(Lj J; m\ M\text{-}m) \right]^2 = D \cdot 1$$

where D is the value of the integral. Also the antisymmetrization factor $\mathscr{A}$ is dropped. Since the product wave function Φ_K (1...A) Φ_A (1...4) was not antisymmetrized, the function shown below should not include an antisymmetrization factor.

$$X_\alpha\ (\xi_A)\ Y_L^m\ (\Omega_{rel})\ \psi_{j\sigma}^{M-m}\ (\xi_K)$$

This neglect of antisymmetrization does not affect the final result.

At this point the problem has been reduced to calculating the expression shown below.

$$G_{jL}^J\ (R_o) = R_o^{\frac{3}{2}} \sum_{\sigma} C_\sigma \int \Phi_{AL}\ (1',2',3',4')\ X_\alpha\ (\xi_\alpha)$$

$$Y_L\ (\Omega_{rel})\ d\ \xi_\alpha\ d\ \Omega_{rel}$$

To evaluate this expression a form for the alpha particle wave function X_α must be selected. The form used by Mang as shown below was also used in this work.

$$X_\alpha(\xi_1, \xi_2, \xi_3, S_1, S_2, S_3, S_4) = X_o^o\ (S_1S_2)\ X_o^o\ (S_3S_4)$$

$$\left(\frac{2\beta^2}{\frac{1}{2}14\pi} \right)^{\frac{3}{2}} \exp\left[-\frac{\beta}{2} \left(\xi_1^2 + \xi_2^2 + \xi_3^2 \right) \right]$$

where

$$\vec{\xi}_1 = \frac{1}{\sqrt{2}} (\vec{r}_1 - \vec{r}_2)$$

$$\vec{\xi}_2 = \frac{1}{\sqrt{2}} (\vec{r}_3 - \vec{r}_4)$$

$$\xi_3 = \frac{1}{2} (\vec{r}_1 + \vec{r}_2 - \vec{r}_3 - \vec{r}_4)$$

S_1, S_2, S_3, S_4 = spin coordinates

X_0^0 = singlet spin function

1,2 refer to protons

3,4 refer to neutrons

$\beta = 0.47/F^2$

$\vec{r}_1$, $\vec{r}_2$, $\vec{r}_3$, $\vec{r}_4$ are radial coordinates of the four nucleons with respect to daughter nucleus

The next step is to transform the wave function $\Phi_{AL}(1',2',3',4')$ from j·j coupling to l·s coupling. This is done by factoring the wave function into single particle wave functions in the following manner.

$$\Phi_{AL}(1',2',3',4') = \left[\left(\Phi_{n_1 j_1}(1)\ \Phi_{n_2 j_2}(2);\ JP\right)\left(\Phi_{n_3 j_3}(3)\ \Phi_{n_4 j_4}(4);JN\right);\ L\right]$$

and by using Fano coefficients[36] to recouple the angular momentum vectors. The resulting expression is

$$\Phi_{(A)L}(1,2,3,4) = \sum_{\substack{LP,SP \\ LN,SN}} \left[(2j_1+1)(2j_2+1)(2j_3+1)(2j_4+1)(2JP+1)(2JN+1)\right]^{\frac{1}{2}}$$

$$X(l_1,\tfrac{1}{2},j_1,l_2,\tfrac{1}{2},j_2,LP,SP,JP)\ X(l_3,\tfrac{1}{2},j_3,l_4,\tfrac{1}{2},j_4,LN,SN,JN)$$

$$\left\{\left[(\Phi_{n_1 j_1}(1')\ \Phi_{n_2 j_2}(2');\ LP)(X_{\frac{1}{2}}X_{\frac{1}{2}};\ SP);\ JP\right]\right.$$
$$\left.\left[(\Phi_{n_3 j_3}(3')\ \Phi_{n_4 j_4}(4');\ LN)(X_{\frac{1}{2}}X_{\frac{1}{2}};\ SP);\ JN\right]\right\};\ L$$

Because the alpha particle wave function contains only spin functions where the proton spins are coupled to SP=0 and the neutron spins are coupled to SN=0, the only terms in the summation in the expression shown above which will contribute to the final result are those with SP=SN=0 and consequently LP=JP, LN=JN. The spin zero functions can be factored out of the wave function and the integral over the spin coordinates performed

$$\int X_0^0 (S_1 S_2) \; (X_{\frac{1}{2}} X_{\frac{1}{2}};\; 0)\; ds_1 ds_2 = 1$$

to bring the expression for $G_{jL}^{J}(R_0)$ into the form

$$G_{jL}^{J}(R_0) = R_0^{\frac{3}{2}} \left(\frac{2\beta^{\frac{3}{2}}}{\pi^{\frac{1}{2}} 4\pi} \right) \sum_{\sigma} C_{\sigma} \int [(2j_1+1)(2j_2+1)(2j_3+1)(2j_4+1)(2JP+1)(2JN+1)]^{\frac{1}{2}}$$

$$X(1_1, \tfrac{1}{2}, j_1, 1_2, \tfrac{1}{2}, j_2, JP, 0, JP)\; X(1_3, \tfrac{1}{2}, j_3, 1_4, \tfrac{1}{2}, j_4, JN, 0, JN)$$

$$Y_L(\Omega_{rel}) \left\{ \left[(\Phi_{n_1 j_1}(1')\; \Phi_{n_2 j_2}(2');\; JP)(\Phi_{n_3 j_3}(3')\; \Phi_{n_4 j_4}(4');\; JN \right];\; L \right\}$$

$$\exp -\frac{\beta}{2} (\xi_1^2 + \xi_2^2 + \xi_3^2)\; \xi_1^2 d\xi_1 \;\; \xi_2^2 d\xi_2 \; \xi_3^2 d\xi_3 \; \xi_4^2 d\xi_4$$

The final series of steps involves transforming the single particle harmonic oscillator wave functions from the oscillator potential basis where they have radial coordinates r_1, r_2, r_3, and r_4 respectively, into wave functions expressed in terms of the relative and center of mass coordinates which were used in the definition of the alpha particle wave function.

$$\xi_1 = \frac{1}{\sqrt{2}} (r_1 - r_2) \qquad \xi_3 = \frac{1}{\sqrt{2}} (\xi_1' - \xi_2')$$

$$\xi_1' = \frac{1}{\sqrt{2}} (r_1 + r_2) \qquad = \frac{1}{2} (r_1 + r_2 - r_3 - r_4)$$

$$\xi_2 = \frac{1}{\sqrt{2}} (r_3 - r_4) \qquad R = \frac{1}{\sqrt{2}} (\xi_1' + \xi_2')$$

$$\xi_2' = \frac{1}{\sqrt{2}} (r_3 + r_4) \qquad = \frac{1}{2} (r_1 + r_2 + r_3 + r_4)$$

This transformation is accomplished in three steps using the method and coefficients defined by Moshinski[37,38]. The first step transforms the proton wave function into a form expressed in terms of ξ_1, the relative coordinate, and ξ_1', the center of mass coordinate. The second step transforms the neutron wave function into a form expressed in terms of ξ_2, the relative coordinate, and ξ_2', the center of mass coordinate.

Each of these tranformations results in a summation of terms as shown below.

$$[\Phi_{n_1 l_1}(r_1,\Omega_1)\ \Phi_{n_2 l_2}(r_2\Omega_2);\ JP] =$$

$$\sum_{\substack{\nu_1\nu_2 \\ \lambda_1\lambda_2}} M \begin{Bmatrix} n_1 l_1 n_2 l_2 JP \\ \nu_1\lambda_1\nu_1'\lambda_1' JP \end{Bmatrix} [\Phi_{\nu_1\lambda_1}(\xi_1,\Omega_{prel})\ \Phi_{\nu_1'\lambda_1'}(\xi_1',\Omega_{pcm});\ JP]$$

$$[\Phi_{n_3 l_3}(r_3,\Omega_3)\ \Phi_{n_4 l_4}(r_4,\Omega_4);\ JN] =$$

$$\sum_{\substack{\nu_3\nu_4 \\ \lambda_3\lambda_4}} M \begin{Bmatrix} n_3 l_3 n_4 l_4 JP \\ \nu_2\lambda_2\nu_2'\lambda_2' JN \end{Bmatrix} \Phi_{\nu_2\lambda_2}(\xi_2,\Omega_{nrel})\ \Phi_{\nu_2'\lambda_2'}(\xi_2,\Omega_{ncm});\ JN]$$

where M represents a Moshinski coefficient.

Only those terms with λ_1 and λ_2 equal to zero will affect the final result though because the integral of the product of a harmonic oscillator wave function $\Phi_{\nu\lambda}(\xi)$ with the term $e^{-\beta/2\,\xi^2}$ from the alpha particle wave function is only non zero for $\lambda=0$.

The third step is to first recouple the wave functions so that

the proton and neutron relative wave functions are coupled together and the proton and neutron center of mass wave functions are coupled together.

$$\left\{\left[\Phi_{\nu_1\lambda_1}(\xi_1,\Omega_{rel}),\ \Phi_{\nu_1'\lambda_1'}(\xi_1',\Omega_{pcm});\ JP\right]\right.$$

$$\left.\left[\Phi_{\nu_2\lambda_2}(\xi_2,\Omega_{rel})\ \ \Phi_{\nu_2'\lambda_2'}(\xi_2',\Omega_{ncm});\ JN\right];\ L\right\} =$$

$$\sum_{\substack{JREL\\JCM}} (2JP+1)(2JN+1)(2JREL+1)(2JCM+1)^{\frac{1}{2}}$$

$$\times\ (\lambda_1,\lambda_1',JP,\lambda_2,\lambda_2',JN,JREL,JLM,L)$$

$$\left\{\left[\Phi_{\nu_1\lambda_1}(\xi_1,\Omega_{prel})\ \Phi_{\nu_2\lambda_2}(\xi_2,\Omega_{nrel});\ JREL\right]\right.$$

$$\left.\left[\Phi_{\nu_1'\lambda_2'}(\xi_1',\Omega_{pcm})\ \Phi_{\nu_2'\lambda_2'}(\xi_2',\Omega_{ncm});\ JCM\right];\ L\right\}$$

Since only terms with $\lambda_1 = \lambda_3 = 0$ need to be considered, the transformation shown above can be simplified. The summation over JREL and JCM is reduced to the one term JCM=1, JREL=0 and the Fano coefficient for this term always has the value one.

$$\left[(2JP+1)(2JN+1)(2L+1)\right]^{\frac{1}{2}} \times (0,JP,JP,0,JN,JN,0,L,L) = 1$$

Then the center of mass part of this wave function is transformed from the coordinates ξ_1' and ξ_2' by a Moshinski transformation to the coordinates ξ_3 and R. As with the proton and neutron transformed wave function only those with an angular momentum value of zero for the relative wave function will contribute to the final result.

The expression for $G_{jL}^{J}(R_o)$ can now be written

$$G_{jL}^{J}(R_o) = R_o^{-\frac{3}{2}} \left(\frac{2\beta^{\frac{3}{2}}}{\frac{1}{2}!4\pi}\right)^{\frac{3}{4}} \sum_{\sigma} C_{\sigma}$$

$$\left[(2j_1+1)(2j_2+1)(2j_3+1)(2j_4+1)(2JN+1)(2JP+1)\right]^{\frac{1}{2}}$$

$$x(l_1,\tfrac{1}{2},j_1,l_2,\tfrac{1}{2},j_2,JP,O,JP)\ x\ (l_3,\tfrac{1}{2},j_3,l_4,\tfrac{1}{2},j_4,JN,O,JN)$$

$$\sum_{\nu_1\nu_2\nu_3 n} M\begin{pmatrix} n_1 l_1 n_2 & l_2 & JP \\ \nu_1 O\ \nu_1' & JP & JP \end{pmatrix} M\begin{pmatrix} n_3 l_3 n_4 & l_4 & JN \\ \nu_2 O\ \nu_2' & JN & JN \end{pmatrix} M\begin{pmatrix} \nu_1 JP\ \nu_2' & JN & L \\ \nu_3\ O\ N & L & L \end{pmatrix}$$

$$\int \Phi_{N,L}(R,\Omega_{rel})\ Y_L(\Omega_{rel})\ d\Omega_{rel}$$

$$\int \Phi_{\nu_1 O}(\xi_1,\Omega_{prel})\ \ell^{-\beta/2\,\xi_1^2}\ \xi_1^2\ d\xi_1\ d\Omega_{prel}$$

$$\int \Phi_{\nu_2 O}(\xi_2,\Omega_{nrel})\ \ell^{-\beta/2\,\xi_2^2}\ \xi_2^2\ d\xi_2\ d\Omega_{nrel}$$

$$\int \Phi_{\nu_3 O}(\xi_3,\Omega_{arel})\ \ell^{-\beta/2\,\xi_3^2}\ \xi_3^2\ d\xi_3\ d\Omega_{arel}$$

For the wave functions $\Phi_{\nu\lambda}(\xi,\Omega)$ harmonic oscillator wave functions as shown below were used.

$$\Phi_{\nu\lambda}(\xi,\Omega) = \alpha^{\frac{3}{2}} \left[\frac{2\nu!}{(\nu+\lambda+\frac{1}{2})!}\right]^{\frac{1}{2}} (\alpha^{\frac{1}{2}}\xi)^{\lambda}$$

$$L_{\nu}^{\lambda+\frac{1}{2}}(\alpha\xi^2)\ \exp(-\tfrac{1}{2}\,\alpha\xi^2)\ Y_{\lambda}(\Omega)$$

where

$\frac{1}{\sqrt{\alpha}} = (\hbar/m\omega)^{\frac{1}{2}}$

$\omega^2 = k/m$

k is the harmonic oscillator potential constant

$L_{\nu}^{\lambda+\frac{1}{2}}(\alpha\xi^2)$ is a Laguerre polynomial

Using the wave functions the angular integrations can be performed

$$\int Y_L^2(\Omega_{rel})\, d\Omega_{rel} = 1$$

and

$$\Pi_i \int Y_0(\Omega_i)\, d\Omega_i = \Pi_i \int \frac{1}{\sqrt{4\pi}}\, d\Omega_i = \left(\frac{4\pi}{\sqrt{4\pi}}\right)^3 = (4\pi)^{\frac{3}{2}}$$

where i = PREL, NREL, AREL

Using this formal expression for $G_{jL}^J(R_o)$, a computer code ALJHA was developed to calculate alpha decay constants. It was run on a CDC 7600 computer where it used 60K of small core memory and 70K of large core memory. The CPU time required to run the program depends on the angular momentum values of the single particle wave functions and the angular momentum of the parent and daughter nuclei. An average value of ~10 seconds of CPU time per configuration was used to calculate the decay constant for the alpha decay of ^{210m}Bi (9-) to ^{206}Tl (2-, 266 keV) using the configuration mixing for ^{206}Tl calculated by Kuo and Herling[39] which includes 16 configurations as shown in Table 19. The ^{210m}Bi(9-) configuration was assumed to be pure $(h_{\frac{9}{2}}^2 g_{\frac{9}{2}}^3;\ 9)$.

The program produces as output on punched cards the value of $G_{jL}^J(R_o)$ for each configuration calculated for a configuration mixed wave function, so that they will not have to be recalculated to determine the alpha decay constant for the decay of the same parent state to other states of the daughter having the same spin and parity, but different linear combinations of the same configurations. This procedure was very useful in reducing the computational costs associated with calculating the alpha decay rates of ^{210m}Bi to the 2- and 1- spin states of ^{206}Tl.

Calculations were conducted for the alpha decay rates of ^{211}Po, ^{211m}Po, ^{210}Bi, and ^{210m}Bi. The results of these calculations are discussed in the next section.

D. Results

1. ^{211}Po, ^{211m}Po

The calculation of the alpha decay constant for the decay of ^{211}Po to ^{207}Pb was conducted to provide a basis for the comparison of the calculations done in this work with those of Zeh and Mang.[4]

The decay scheme for ^{211}Po is shown in Fig. 18. Alpha decay of the ^{211}Po ($\frac{9}{2}^+$, g.s) has been observed[40-45] as shown to the ground state and to the first two excited states of ^{207}Pb. Alpha decay to the third excited state was reported by Neuman and Perlman[40] but was not seen by Galovkove et al.[45], who set an upper limit for this branching ratio of .002%.

The present calculation was conducted using the normalized wave function for the ^{211}Po ground state given by Zeh and Mang[4]. Pure harmonic oscillator wave functions were used for ^{207}Pb instead of the wave functions of Bloomquest and Wahlborn[46]. The harmonic oscillator constant α was set equal to $0.17 \times 10^{26}/cm^2$ and the alpha particle wave function constant β was set equal to $0.47 \times 10^{26}/cm^2$. The radius chosen for the calculation was 9.0 Fermis. All of these parameters were chosen to agree with those used by Zeh and Mang.

A comparison of the results of the present calculation and those of Zeh and Mang is shown in Tables 15 and 16. The relative decay rates of ^{211}Po to the $\frac{5}{2}^-$ and $\frac{3}{2}^-$ of ^{207}Pb as calculated in this work were slightly less than twice the values calculated by Zeh and Mang, but this

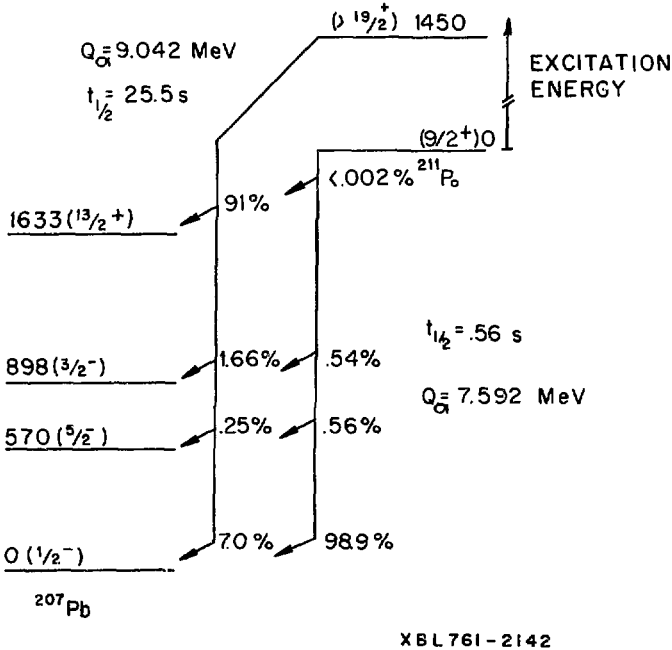

Figure 18. Decay scheme of ^{211}Po.

Table 15. Relative Alpha Decay Rates for ^{211}Po

^{207}Pb Level	Present	Zeh & Mang	Exp[b]
1/2 -	1 [a]	1 [a]	1
5/2 -	.0045	.0079	.0053
3/2 -	.0025	.0047	.0050
13/2 +	5×10^{6}	--	--

(a) Normalized to 1. The calculated absolute values are orders of magnitude lower than experimentally measured alpha decay rates.

(b) Reference 30.

Table 16. Alpha Particle Angular Momentum (L) Contributions to the ^{211}Po Alpha Decay Rate

^{207}Pb Level	L	Relative Alpha Decay Rates Present	Zeh & Mang
1/2 -	5	1	1
5/2 -	3	1	1
	5	.85	.81
	7	.42	.37
3/2 -	3	1	1
	5	.12	.12

discrepancy was not considered significant.* Excellent agreement was obtained for the ratios between the alpha decay rates for different values of alpha particle center of mass angular momentum L.

The dependence of the alpha decay constant of ^{211}Po on the radial parameter R_o was measured by calculating the relative decay constants at several values of R_o ranging from 7.0 F to 9.5 F. The results shown in Table 17 agree with Zeh and Mang's results in that the values are only slowly varying if not constant over the radial range considered. The data point 7.5 F is significant in that the maximum value of $R \cdot G_{\frac{1}{2}\,5}^{9/2}(R)$ occurs at that radius as shown in Fig. 19.

An area where a large disagreement occurred between values calculated in this work and those of Zeh and Mang was the absolute value for the alpha decay constant of ^{211}Po. At 9.0 F Zeh and Mang calculate the ^{211}Po alpha decay constant as 6.5×10^{6} sec^{-1} while in this work the value at 9.0 F was calculated as 4.6×10^{7} sec^{-1}. No source for this discrepancy could be found. Note that both values are in extreme error when compared to the experimentally measured value of 1.33 sec^{-1}. Recently Fliessbach[47] has presented evidence that a renormalization of the alpha particle nucleus wave function will bring the calculated results into better agreement with the experimentally measured values.

Table 17. Variation of the Calculated Alpha Branching Ratios of ^{211}Po with R

Spin of ^{211}Po State	R = 7.0	7.3	7.5	8.0	8.5	9.0	9.5
1/2-	99.1	99.2	99.2	99.3	99.3	99.3	99.3
5/2-	.63	.56	.51	.45	.43	.41	.40
3/2-	.23	.24	.24	.24	.25	.25	.25

*Especially since Mang used "realistic radial functions" for ^{207}Pb and pure harmonic oscillator wave functions were used in this work.

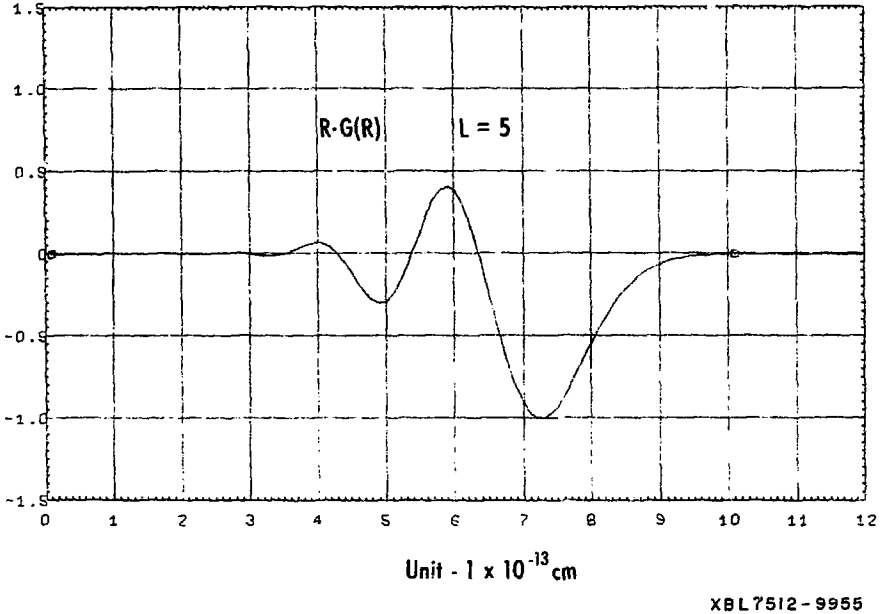

Figure 19. R • G(R) for the alpha decay ^{211}Po (9/2+) → ^{207}Pb (1/2-).

Alpha decay of the metastable 1.45 MeV excited state of ^{211}Po has been observed[48], as shown in Fig. 18 to the ground state and first three excited states of ^{207}Pb. The spin of this metastable state is thought to be greater than 19/2 based on Weisskopf single particle estimates of transition rates of this level to the ground state.

Alpha decay constants were calculated for the alpha decay of ^{211m}Po for several different harmonic oscillator wave functions. The calculations used a radius of 9 F and $0.17/F^2$, $0.47/F^2$ for alpha and beta respectively. The results are shown in Table 18.

Table 18. Relative Alpha Decay Rates for ^{211m}Po

	Decay to ^{207}Pb($\frac{1}{2}$-)			^{207}Pb Level	
^{211m}Po Configuration	^{211m}Po/^{211}Po	$\frac{1}{2}$-	$\frac{5}{2}$-	$\frac{3}{2}$-	$\frac{13}{2}$+
$[(h\frac{9}{2})^2\ 8;\ g\frac{9}{2}]\frac{21}{2}$+	.17	1	.037	.045	.0038
$[(h\frac{9}{2})^2\ 8;\ g\frac{9}{2}]\frac{23}{2}$+	.023	1	.20	.0011	4×10^{5}
$[(h\frac{9}{2})^2\ 8;\ g\frac{9}{2}]\frac{25}{2}$+	.016	1	.052	.062	.017
$[(h\frac{9}{2})^2\ 8;\ i\frac{11}{2}]\frac{27}{2}$+	.0081	1	.27	.001	10^{4}
$[(h\frac{9}{2})(f\frac{7}{2})\ 8;\ g\frac{9}{2}]\frac{25}{2}$+	.14	1	.053	.062	.017
$[(h\frac{9}{2})(f\frac{7}{2})\ 8;\ i\frac{11}{2}]\frac{27}{2}$+	.073	1	.28	.001	10^{3}
Experiment[a]	.0016	1	.036	.24	13

[a] Reference 37.

The agreement with experimentally measured relative alpha decay rates was much worse for this case as compared to the ^{211}Po ground state. The ratio of ^{211m}Po to ^{211}Po calculated alpha decay rates for the decay to the ^{207}Pb ground state was in all cases higher than the experimental value. The calculated relative alpha decay rates of ^{211m}Po to the second and third excited states as compared to ^{211m}Po decay to the ^{207}Pb ground state were too low in all cases. This discrepancy was particularly bad for the $(\frac{13}{2}+)$ level of ^{207}Pb for which the calculated relative alpha decay rate was for the best case a factor of ~800 lower than the experimental value. Zeh and Mang also observed this discrepancy in their calculations and hypothesized that the enhancement of the alpha decay of ^{211m}Po to ^{207}Pb $(\frac{13}{2}+)$ is due to the presence of terms in the ^{211m}Po wave function where a neutron vacancy exists in the $i\frac{13}{2}$ shell and two $g\frac{9}{2}$ neutrons exist.*

2. ^{210}Bi, ^{210m}Bi

The alpha decay of the ^{210}Bi (1-) ground state to levels of ^{206}Tl was not studied experimentally in this work but has been previously observed[6] to the first two excited states of ^{206}Tl. A diagram of the states of ^{206}Tl can be seen in Fig. 20.

The ratio of the alpha decay constants for the decay of ^{210}Bi to the 266 keV and 305 keV excited states of ^{206}Tl was calculated using a radius 9.0 F, $\alpha = 0.17/F^2$, and $\beta = 0.47/F^2$. The wave function used for the ^{210}Bi (1-) state was $[h\frac{9}{2}, g\frac{9}{2}; 1-]$, while for ^{206}Tl the configuration mixed wave functions of Kuo and Herling[39], shown in Table 19, were used.

---

* $[(h\frac{9}{2})^2_{jp}, (g\frac{9}{2})^2_{jm}, (i\frac{13}{2})^{-1}]_{Jf}$

Table 19. ^{206}Tl Wave Functions (Approx. #3, Kuo and Herling[39])

Configuration				Tl Excited States							
				266 keV	305 keV	635 keV	650 keV	801 keV	952 keV	998 keV	1120 keV
				2-	1-	2-	1-	3-	4-	2-	1-
Og $\frac{7}{2}$		Oh $\frac{9}{2}$		+.020	+.025	-.012	-.062	+.021	+.025	+.016	+.058
Og $\frac{7}{2}$		1f $\frac{7}{2}$		+.015	-.009	-.018	+.024	-.007	+.014	-.010	-.009
Og $\frac{7}{2}$		1f $\frac{5}{2}$		+.042	-.006	+.000	-.003	+.005	+.038	+.017	+.021
Og $\frac{7}{2}$		2p $\frac{3}{2}$		+.035	—	-.023	—	+.006	+.019	+.007	—
Og $\frac{7}{2}$		2p $\frac{1}{2}$		—	—	—	—	-.017	+.056	—	—
1d $\frac{5}{2}$		Oh $\frac{9}{2}$		-.037	—	+.036	—	+.021	-.018	-.015	—
1d $\frac{5}{2}$		1f $\frac{7}{2}$		-.041	+.001	-.034	-.130	+.035	-.007	-.072	+.113
1d $\frac{5}{2}$		1f $\frac{5}{2}$		-.051	+.038	+.124	-.057	+.126	-.093	+.014	+.035
1d $\frac{5}{2}$		2p $\frac{3}{2}$		-.088	+.042	-.047	-.052	+.041	-.063	-.146	+.033
1d $\frac{5}{2}$		2p $\frac{1}{2}$		+.016	—	+.032	—	+.159	—	+.281	—
1d $\frac{3}{2}$		Oh $\frac{9}{2}$		—	—	—	—	+.067	+.033	—	—
1d $\frac{3}{2}$		1f $\frac{7}{2}$		-.002	—	-.156	—	+.038	+.092	-.119	—
1d $\frac{3}{2}$		1f $\frac{5}{2}$		+.230	+.141	-.148	-.259	+.172	+.984	+.213	+.536
1d $\frac{3}{2}$		2p $\frac{3}{2}$		+.109	-.558	-.100	+.274	+.194	—	-.156	+.216
1d $\frac{3}{2}$		2p $\frac{1}{2}$		+.860	-.109	+.073	-.822	—	—	-.446	+.389
2s $\frac{1}{2}$		Oh $\frac{9}{2}$		—	—	—	—	—	-.039	—	—
2s $\frac{1}{2}$		1f $\frac{7}{2}$		—	—	—	—	-.027	+.020	—	—
2s $\frac{1}{2}$		1f $\frac{5}{2}$		-.323	—	+.640	—	+.936	—	-.572	—
2s $\frac{1}{2}$		2p $\frac{3}{2}$		-.267	-.153	-.712	-.262	—	—	-.527	+.664
2s $\frac{1}{2}$		2p $\frac{1}{2}$		—	+.960	—	-.124	—	—	—	-.035
Oh $\frac{11}{2}$		Oi $\frac{13}{2}$		+.054	-.016	+.020	+.246	-.061	+.023	+.080	-.173

A comparison of the calculated ratio to the experimentally measured ratio is shown in Table 20. The calculated value was a factor of 2.5 lower than the experimental value.

This ratio between decay rates to the first two excited states of ^{206}Tl was also calculated without using configuration mixed wave functions. The results of these calculations are displayed in Table 21 where the wave function used for the 266 keV (2-) excited state is displayed on the vertical axis and the wave function used for the 305 keV (1-) excited state is displayed on the horizontal axis. Several different combinations of wave functions reproduce the experimental value for the ratio of alpha decays of ^{210}Bi (1-) to these excited states of ^{206}Tl.

The alpha decay of ^{210m}Bi (9-) was observed in this work to eight excited states of ^{206}Tl as shown in Fig. 20. The alpha decay constants for these transitions were calculated using the same parameters used in the calculation of ^{210}Bi (1-) ground state alpha decay rates. The wave functions of Kuo and Sterling as shown in Table 19 were used for the ^{206}Tl states while for the ^{210m}Bi state a pure $(h_{\frac{9}{2}}\, g_{\frac{9}{2}};\ 9^-)$ harmonic oscillator configuration was used. The results of these calculations are shown in Table 22.

Table 20. Ratio of ^{210}Bi (1-) Decay Rates

^{206}Tl Wave Function		305 (1-) / 266 (2-)
2-	1-	
Exp[a]	Exp[a]	1.5
Conf Mixed[b]	Conf Mixed[b]	.58

[a] Reference 6

[b] Wave Functions shown in Table 19.

Table 21. Ratio of ^{210}Bi (1-) Alpha Decay Rates for Pure Harmonic Oscillator States

266 keV W.F. \ 305 keV W.F.	$g_{7/2}h_{9/2}$	$g_{7/2}f_{7/2}$	$g_{7/2}f_{5/2}$	$d_{5/2}f_{7/2}$	$d_{5/2}f_{5/2}$	$d_{5/2}p_{3/2}$	$d_{3/2}f_{5/2}$	$d_{3/2}p_{3/2}$	$d_{3/2}p_{1/2}$	$s_{1/2}p_{3/2}$	$s_{1/2}p_{1/2}$	$h_{11/2}i_{13/2}$
$g_{7/2}h_{9/2}$	0.7	5.3	2.6	8.5	12.5	8.2	4.7	16.0	5.8	8.8	14.2	2.1
$g_{7/2}f_{7/2}$	All $> 10^{10}$ ----------------											
$g_{7/2}f_{5/2}$	0.3	1.8	0.9	3.0	4.4	2.9	1.6	5.6	2.0	3.1	5.0	0.7
$g_{7/2}p_{3/2}$	0.2	1.4	0.7	2.3	3.4	2.2	1.3	4.4	1.6	2.4	3.8	0.6
$d_{5/2}h_{9/2}$	0.3	2.0	1.0	3.2	4.7	3.1	1.8	6.1	2.2	3.3	5.8	0.3
$d_{5/2}f_{7/2}$	0.1	0.6	0.2	0.9	1.3	0.9	0.5	1.7	0.6	1.0	1.5	0.2
$d_{5/2}f_{5/2}$	All $> 10^{10}$ ----------------											
$d_{5/2}p_{3/2}$	0.05	0.4	0.2	0.7	1.0	0.7	0.4	1.3	0.5	0.7	1.1	0.2
$d_{5/2}p_{1/2}$	0.1	0.7	0.4	1.2	1.8	1.2	0.7	2.3	0.8	1.3	2.0	0.3
$d_{3/2}f_{7/2}$	0.1	0.8	0.4	1.2	1.8	1.2	0.7	2.3	0.8	1.3	2.0	0.3
$d_{3/2}f_{5/2}$	0.1	0.7	0.4	1.2	1.7	1.2	0.7	2.3	0.8	1.2	2.0	0.3
$d_{3/2}p_{3/2}$	All $> 10^{10}$ ----------------											
$d_{3/2}p_{1/2}$	0.1	0.5	0.2	0.8	1.2	0.8	0.4	1.5	0.5	0.8	1.3	0.2
$s_{1/2}f_{5/2}$	0.1	0.9	0.4	1.4	2.1	1.4	0.8	2.7	1.0	1.5	2.4	0.3
$s_{1/2}p_{3/2}$	0.05	0.3	0.2	0.5	0.8	0.5	0.3	1.0	0.4	0.6	0.9	0.1
$h_{11/2}i_{13/2}$	0.2	1.7	0.8	2.7	3.9	2.6	1.5	5.1	1.8	2.8	4.5	0.7

Table 22. ^{210m}Bi (9-) Alpha Decay Rates

^{206}Tl level	Spin (π)	Exp	Conf[a] Mixed	Branching Ratios Pure H.O.		Conf[b] Mixed	
266	2-	56	85.9	$s_{\frac{1}{2}} f_{\frac{5}{2}}$	69	$.98(s_{\frac{1}{2}} f_{\frac{5}{2}}) - .17(s_{\frac{1}{2}} p_{\frac{3}{2}})$	50
305	1-	39	12.3	$s_{\frac{1}{2}} p_{\frac{1}{2}}$	27	$s_{\frac{1}{2}} p_{\frac{1}{2}}$	45
635	2-	1.4	.045	$s_{\frac{1}{2}} p_{\frac{3}{2}}$	1.1	$-.17(s_{\frac{1}{2}} f_{\frac{5}{2}}) + .98(s_{\frac{1}{2}} p_{\frac{3}{2}})$	1.2
650	1-	5.9	1.74	$d_{\frac{3}{2}} p_{\frac{3}{2}}$	2.4	$d_{\frac{3}{2}} p_{\frac{1}{2}}$	4.0
801	3-	.21	.028	$s_{\frac{1}{2}} f_{\frac{5}{2}}$	.0084	$.93(s_{\frac{1}{2}} f_{\frac{5}{2}}) + .37(s_{\frac{1}{2}} f_{\frac{7}{2}})$	.5
952	4-	.006	.0026	$d_{\frac{3}{2}} f_{\frac{5}{2}}$	.011	$d_{\frac{3}{2}} f_{\frac{5}{2}}$	.019
998	2-	.0008	.00087	$d_{\frac{3}{2}} p_{\frac{1}{2}}$	.002	$d_{\frac{3}{2}} p_{\frac{1}{2}}$	.005
1120	1-	.002	.00012	$s_{\frac{1}{2}} p_{\frac{3}{2}}$	.002	$s_{\frac{1}{2}} p_{\frac{3}{2}}$	.005

[a] Wave functions of Reference 38.

[b] Calculated as described in the text to fit experimental data.

The agreement between the calculated and measured values is only fair. The calculated branching ratio to the first 2- level of ^{206}Tl at 266 keV is high while the calculated branching ratio to the second 2- level at 635 keV is too low by a factor of 7. The calculated branching ratios for the first two 1- levels are both low, but the ratio between them is correct. The branching ratio to the 3- level at 801 keV is low by a factor of 10, but agreement is fairly good for the 4- level at 952 keV and the 2- level at 998 keV. The calculated branching ratio for the 1- level at 1120 keV was low by a factor of 20.

As with ^{210}Bi (1-) the calculation was also done using pure harmonic oscillator wave functions for ^{206}Tl. The results of these calculations for the first five excited states of ^{206}Tl are shown in Table 23.

The experimental value for the ratio of the alpha decay rates to the 266 keV (2-) and 635 keV (2-) ^{206}Tl levels was best approximated by using the configuration $(s_{\frac{1}{2}}, f_{\frac{5}{2}}; 2^-)$ for the 266 keV level and $(s_{\frac{1}{2}}, p_{\frac{3}{2}}; 2^-)$ for the 635 keV level, but the calculated value was still too low as shown in Table 23. The correct ratio was reproduced by introducing configuration mixing between the two configurations $(s_{\frac{1}{2}}, f_{\frac{5}{2}}; 2^-)$ and $(s_{\frac{1}{2}}, p_{\frac{3}{2}}; 2^-)$. Two sets of configuration mixed wave functions calculated to give the correct ratio between the alpha decay rates to the 266 keV level and the 635 keV level were calculated.

^{206}Tl (266 keV, 2-) $\quad .98(s_{\frac{1}{2}} f_{\frac{1}{2}}) - .17(s_{\frac{1}{2}} p_{\frac{3}{2}})$

^{206}Tl (635 keV, 2) $\quad -.17(s_{\frac{1}{2}} f_{\frac{1}{2}}) + .98(s_{\frac{1}{2}} p_{\frac{3}{2}})$

and

^{206}Tl (266 keV, 2-) $\quad .75(s_{\frac{1}{2}} f_{\frac{1}{2}}) - .5(s_{\frac{1}{2}} p_{\frac{3}{2}})$

^{206}Tl (635 keV, 2-) $\quad -.5\ (s_{\frac{1}{2}} f_{\frac{1}{2}}) + .75(s_{\frac{1}{2}} p_{\frac{3}{2}})$

Column three in Table 22 was calculated using the first set of configuration mixed wave functions. Calculations with the second set gave a value for the decay rate to the 266 keV excited state which was a factor of 50 too low when compared to the calculated alpha decay rate of ^{210m}Bi to the 305 keV excited state.

Configuration mixed wave functions were also calculated using the $(d_{\frac{3}{2}} p_{\frac{1}{2}}; 2^-)$ configuration mixed with either the configuration $(s_{\frac{1}{2}} f_{\frac{5}{2}}; 2^-)$ or $(s_{\frac{1}{2}} p_{\frac{3}{2}}; 2^-)$ but for both cases the wave functions calculated to produce the correct ratio between the alpha decay rates of ^{210m}Bi to the 635 keV and 266 keV excited states of ^{206}Tl gave decay rates for the 266 keV

Table 23. Relative Alpha Decay Rates of ^{210m}Bi (9·) to Levels of ^{206}Tl Calculated Using Pure Harmonic Oscillator Wave Functions

Wave Function	266 keV level(2-)	305 keV level(1-)	635 keV level(2-)x10^3	650 keV level(1-)x10^2	801 keV level(3-)x10^3
$h\frac{11}{2}i\frac{13}{2}$	.22	.23	1.5	.18	2.7
$g\frac{7}{2}h\frac{9}{2}$	.15	.10	.93	.73	2.9
$g\frac{7}{2}f\frac{7}{2}$	10^{15}	.89	10^{15}	.70	4.0
$g\frac{7}{2}f\frac{5}{2}$	.43	1.9	2.7	1.5	2.3
$g\frac{7}{2}p\frac{3}{2}$	.57	–	3.5	–	5.9
$g\frac{7}{2}p\frac{1}{2}$	–	–	–	–	8.4
$d\frac{5}{2}h\frac{9}{2}$	.40	–	2.5	–	.41
$d\frac{5}{2}f\frac{7}{2}$	1.39	6.3	8.7	5.0	7.5
$d\frac{5}{2}f\frac{5}{2}$	10^{14}	.82	10^{14}	.65	.80
$d\frac{5}{2}p\frac{3}{2}$	1.89	1.1	12.0	.81	2.7
$d\frac{5}{2}p\frac{1}{2}$	1.06	–	6.2	–	.14
$d\frac{3}{2}h\frac{9}{2}$	–	–	–	–	.10
$d\frac{3}{2}f\frac{7}{2}$	1.03	–	6.4	–	10.4
$d\frac{3}{2}f\frac{5}{2}$	1.07	.62	6.6	.46	1.5
$d\frac{3}{2}p\frac{3}{2}$	10^{15}	3.7	10^{15}	2.9	32.4
$d\frac{3}{2}p\frac{1}{2}$	1.59	4.3	9.8	3.4	–
$s\frac{1}{2}f\frac{7}{2}$	–	–	–	–	23.4
$s\frac{1}{2}f\frac{5}{2}$	.98	–	5.7	–	.12
$s\frac{1}{2}p\frac{3}{2}$	2.41	6.6	15	5.2	–
$s\frac{1}{2}p\frac{1}{2}$	–	.38	–	.25	–
Barrier Pen[a] for Lowest L	1 (L=8)	.63 (L=8)	.0062 (L=8)	.0042 (L=8)	.00583 (L=6)

[a] Normalized to the value for L=8 and 4.946 MeV

excited state that were too low by a factor greater than 10 when compared to the decay rate of ^{210m}Bi to the 305 keV excited state of ^{206}Tl using the configuration $(s_{\frac{1}{2}}\, p_{\frac{1}{2}};\ 1^-)$.

The experimentally measured ratio between the alpha decay rates to the 305 keV and 650 keV levels of ^{206}Tl was best reproduced by using the configuration $(s_{\frac{1}{2}} p_{\frac{1}{2}};\ 1^-)$ for the 305 keV level and $(s_{\frac{1}{2}}\, p_{\frac{3}{2}};\ 1^-)$ for the 650 keV level. All other choices of configurations for the 305 keV (1^-) level result in values for the ratio that are too low, particularly for the configurations $(s_{\frac{1}{2}}\, p_{\frac{3}{2}})$, $(d_{\frac{3}{2}}\, p_{\frac{1}{2}})$, and $(d_{\frac{3}{2}}\, p_{\frac{3}{2}})$ for which the ratio is too low by factors of more than 10. This indicates that the predominate character of the 305 keV level of ^{206}Tl is $(s_{\frac{1}{2}}\, p_{\frac{1}{2}})$.

For the 801 keV level of ^{206}Tl the branching ratio calculated using the configuration $(s_{\frac{1}{2}}\, f_{\frac{5}{2}};\ 3^-)$ was too low by an order of magnitude. Using the configuration $(s_{\frac{1}{2}}\, f_{\frac{7}{2}};\ 3^-)$ results in a value that is too high by a factor of ten. The amount of configuration mixing between these two configurations needed to produce the correct branching ratio was calculated and is shown below.

$$^{206}\text{Tl (801 keV, 3}^-\text{)} \qquad .95(s_{\frac{1}{2}}\, f_{\frac{5}{2}}) + .37(s_{\frac{1}{2}}\, f_{\frac{7}{2}})$$
$$\text{or} \quad .97(s_{\frac{1}{2}}\, f_{\frac{5}{2}}) - .26(s_{\frac{1}{2}}\, f_{\frac{7}{2}})$$

As discussed in Chapter II, Section B, alpha decay of ^{210m}Bi (9$^-$) is forbidden to the ground state of ^{206}Tl (0$^-$) because the alpha particle must carry off 9 units of angular momentum (L=9), and for L values which are odd number the parent and daughter states must be of opposite parity. Only if a slight amount of a positive parity configuration is mixed into either the ^{210m}Bi or ^{206}Tl ground state wave function can this alpha decay occur.

The admixture of a positive parity wave function into the ^{206}Tl ground state is unlikely because no combination of a proton hole with a neutron hole can be formed with spin and parity 0+ by using proton and neutron hole states with energies less than 3.5 MeV below the closed shell energy.

Two positive parity configurations that could mix into the ^{210m}Bi (9-) wave function are

$$(1)\quad i\,\tfrac{13}{2}\;g\,\tfrac{9}{2}$$

$$\text{or}\quad (2)\quad h\,\tfrac{9}{2}\;j\,\tfrac{15}{2}$$

The alpha decay rate of ^{210m}Bi (9+) was calculated using the same parameters used previously with ^{210m}Bi and the results of these calculations are shown in Table 24. The minimum amount of parity mixing was calculated by equating the calculated and experimental values. This minimum value is a limit on the extent of parity mixing in the wave function of ^{210m}Bi (9-).

Table 24. ^{210m}Bi (9+) Relative Alpha Decay Rates

Configuration		Branching Ratio		
^{210m}Bi	^{206}Tl	Calc[b]	Exp	a x 10^4[a]
$i\,\frac{13}{2}\;g\,\frac{9}{2}$; 9+	$s\,\frac{1}{2}\;p\,\frac{1}{2}$; 0-	a^2 6083	<10^{-4}	<1.3
$i\,\frac{13}{2}\;g\,\frac{9}{2}$; 9+	$d\,\frac{3}{2}\;p\,\frac{3}{2}$; 0-	a^2 8097	<10^{-4}	1.1
$h\,\frac{9}{2}\;j\,\frac{13}{2}$; 9+	$s\,\frac{1}{2}\;p\,\frac{1}{2}$; 0-	a^2 1105	<10^{-4}	5.0
$h\,\frac{9}{2}\;j\,\frac{13}{2}$; 9+	d – p – ; 0-	a^2 1472	<10^{-4}	2.6

[a] Based on Column 2 of Table 23.

[b] Calculated by equating the experimental and calculated values.

IV. Conclusions

In the second chapter of the work the results of various spectroscopic measurements conducted with ^{210m}Bi sources were presented but very little attention was given to the relationships between the results of the different spectroscopic measurements and to the description of a decay scheme for ^{210m}Bi. Those tasks were reserved for this chapter. The decay scheme of ^{210m}Bi will be presented and discussed and the spectroscopic information pertaining to each of the states of ^{206}Tl will be reviewed and summarized.

The decay scheme of ^{210m}Bi as measured in this work is shown in Fig. 20. For comparison a diagram of the levels of ^{206}T observed by several different experimental methods[49-53] is given in Fig. 21. Also included in Fig. 21 is a diagram of the levels of ^{206}Tl as calculated by Kuo and Herling.[39]

No alpha decay of ^{210m}Bi was observed to the ground state of ^{206}Tl which is consistent with the measurement by Cussins et al.[55] of the spin of this state as zero since the alpha decay of ^{210m}Bi (9-) to a state with zero spin and negative parity is forbidden as discussed in Chapter II Section B1c.* The assignment of zero spin and negative parity is further supported by the E2 character of the 265.6 keV transition between the first excited state and the ground state of ^{206}Tl. The E2 character of this transition was observed in the internal conversion electron spectrum as shown in Table 12. The most probable shell model configuration for this state is $(s\frac{1}{2}\ p\frac{1}{2};\ 0)$. A diagram of the neutron and proton single particle shell model levels around the closed proton shell at Z=82 and the closed neutron shell at N=126 is shown in Fig. 22.

---

*The possible extent of parity violation is discussed in Chapter III Section D2.

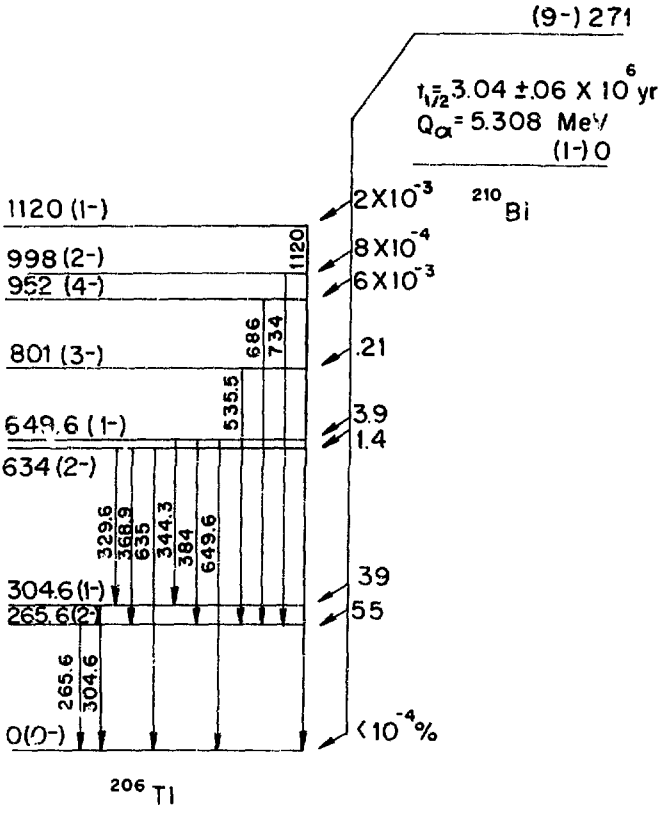

Figure 20. Decay scheme of ^{210m}Bi.

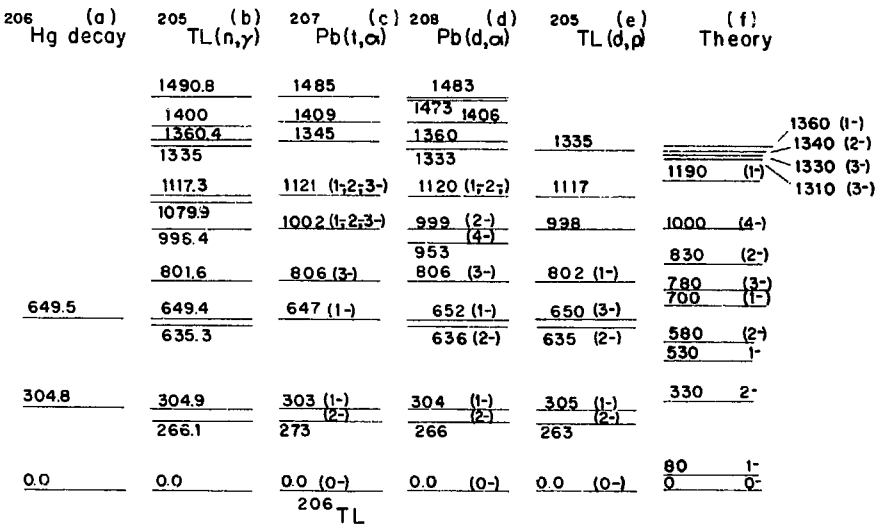

XBL761-2144

Figure 21. Energy levels of ^{206}Tl.
(a) Ref. 49 (d) Ref. 52
(b) Ref. 50 (e) Ref. 51
(c) Ref. 53 (f) Ref. 39

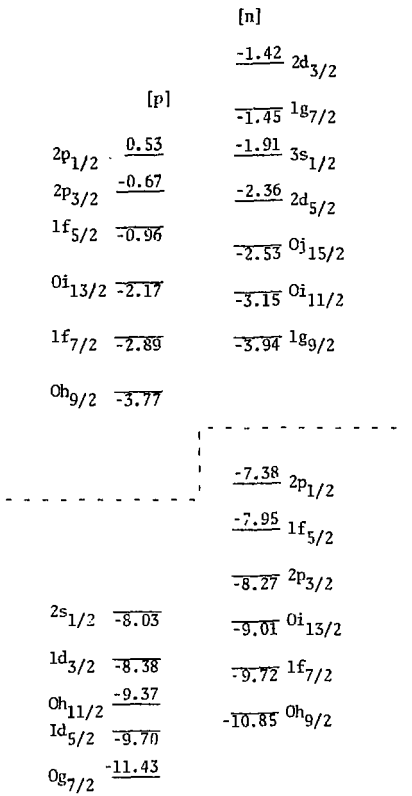

Fig. 22 Single particle neutron and p states near closed shell N = 126, Z = 82.

The first excited state of ^{206}Tl observed in this work was at 265.6 ± .2 keV. This energy is based on the gamma ray energy for the transition between this state and the ground state as shown in Table 7. The alpha branch leading to the 265.6 keV excited state was identified in alpha-gamma coincidence experiments where a strong coincidence was observed between an alpha particle with an energy of 4.946 ± .001 MeV* and a 266 keV gamma ray. The intensity of this alpha branch was measured as 56 ± 1% in alpha-gamma coincidence measurements and 55 ± 1% in alpha singles measurements.

Confirmation that the 4.946 MeV alpha decay of ^{210m}Bi leads directly to the 265.6 keV excited state of ^{206}Tl was obtained by checking the A=210, 206 α,β decay cycle, a diagram of which is shown in Fig. 23. The total energy for the two sides agrees within experimental error. The E2 character of the 266 keV transition discussed earlier supports the assignment of a spin of 2 to this level.

The results of calculations of the branching ratio to this excited state of ^{206}Tl using several different wave functions are shown in Table 22. On the basis of the single particle energy levels shown in Fig. 22, the predominant configuration in the wave function for this excited state should be $(d\frac{3}{2}\ p\frac{1}{2};\ 2^-)$ but the best agreement between calculated and experimental values was obtained using the configuration $(s\frac{1}{2}\ f\frac{5}{2};\ 2^-)$.

Alpha branching to a 304.6 ± .2 keV excited state of ^{206}Tl was observed in alpha singles measurements with an energy 4.909 ± .001 MeV and an alpha branching ratio of 39.5 ± .8%. In alpha-gamma coincidence measurements a coincidence peak involving the 4.909 MeV alpha and the 305 keV gamma was observed with an intensity which was calculated to

*This energy value was measured using an alpha singles spectrum.

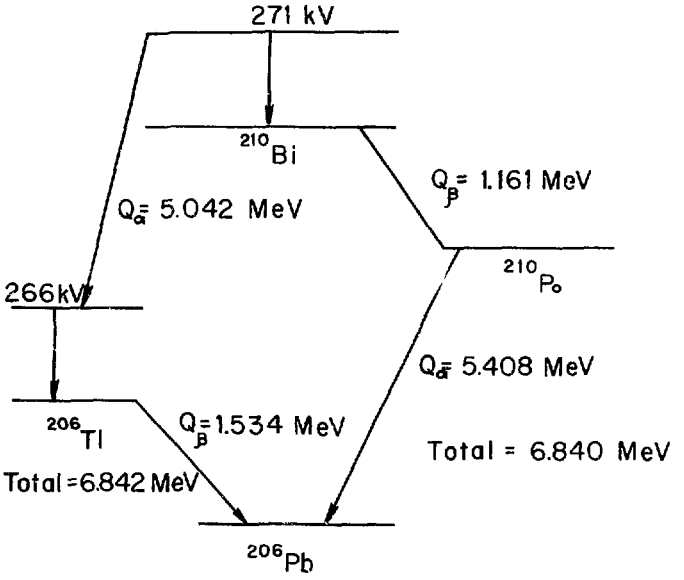

Figure 23. A = 210,206 alpha, beta decay cycle.

correspond to an alpha branching ratio of 38.8 ± .7%. No coincidence was observed involving the 4.909 MeV alpha and the 266 keV gamma. Conversion electron measurements indicate that the 304.6 keV transition is M1 which in turn indicates that the spin of this excited state is one. Calculations of the alpha branching to the 304.6 keV excited state of ^{206}Tl shown in Tables 22 and 23 indicate that the predominate configuration in the wave function for this excited state is $(s\frac{1}{2}\, p\frac{1}{2};\ 1^-)$.

The third excited state of ^{206}Tl observed in this study of the alpha decay of ^{210m}Bi had an excitation energy of 634.2 ± .3 keV. The energy of the alpha decay leading to this excited state was measured as 4.584 ± .002 MeV in alpha-gamma coincidence measurements. In alpha singles spectra the 4.584 MeV alpha peak could not be resolved from an alpha peak with energy 4.569 ± .002 MeV. The alpha branching ratio to this excited state of ^{206}Tl was calculated using alpha-gamma coincidence intensities as 1.4 ± .1%.

Five gammas were observed in coincidence with the 4.584 alpha. Their energies were 266, 305, 330, 369, and 635 keV. These coincidences occur when the 634.2 keV excited state of ^{206}Tl gamma decays to the 266 keV or 305 keV excited states or to the ground state of ^{206}Tl. Confirmation that the 330 keV and 369 keV gammas were produced by the transitions from the 634.2 keV excited state to the 304.6 keV and 265.6 kev excited states, respectively, was obtained by gamma gamma coincidence measurements. Coincidences were observed between the 266 and 369 keV gammas and between the 305 and 330 keV gammas. Conversion electron measurements indicated that the 329.6 keV and 368.9 keV transitions were M1 but the conversion electron intensities for the 635 keV transition were too low to be observed. The M1 character of the 329.6 keV

transition from the 634.2 keV excited state to the 304.6 keV excited state of ^{206}Tl which has a spin and parity 1-, indicates that the spin of the 634.2 keV excited state is 0, 1 or 2 and its parity is negative. Since the alpha decay of ^{210m}Bi (9-) to a state of ^{206}Tl with spin and parity 0- is parity forbidden, the spin 0 possibility can be ignored. Also, if the spin of the 634.2 keV excited state were zero, the multipolarity of the 368.9 keV transition would be E2 instead of M1. The ratios between the relative intensities for a 635 keV E2 gamma and a 369 keV M1 gamma were calculated using Weiskopf single particle formulas.[24] The calculated ratio of .012 agreed fairly well with the experimentally measured ratio of .016. This same ratio calculated between a 635 keV M1 gamma and a 369 keV M1 gamma was 5.10. Based on these comparisons of calculated relative gamma intensity ratios to the measured values, a spin of 2 was assigned to the 635 keV excited state of ^{206}Tl.

Alpha decay of ^{210m}Bi to an excited state of ^{206}Tl at 649.6 ± .2 keV was observed with a branching ratio of 3.9 ± .1% in alpha-gamma coincidence measurements. The energy for the alpha decay was measured as 4.568 ± .002 MeV. Three gammas with energies 305, 344, and 650 keV were observed in coincidence with the 4.56[illegible] MeV alpha. The 344 is produced by a transition from the 649.6 keV excited state to the 305 keV excited state of ^{206}Tl. The coincidence between 305 and 344 keV gammas was observed in gamma-gamma coincidence measurements. The 650 keV gamma is produced by the decay of the 649.6 keV excited state to the ground state of ^{206}Tl. A 384 keV gamma produced by the transition from the 649.6 keV excited state to the 305 keV excited state of ^{206}Tl was observed in gamma singles measurements with a relative intensity of .011%, but was not observed in alpha-gamma coincidence measurements where an intensity of .01% would have been obscured by background. Internal conversion electron

measurements indicated that the 344 and 650 keV gammas were M1, and the experimentally measured ratio, 5.5, of the intensity of the 650 keV gamma to the 344 keV gamma agrees with the value, 5.2, calculated using the Weiskopf formula to calculate transition rates for a 369 keV M1 gamma and a 650 keV M1 gamma. Based on these indications that the 649.6 keV gamma transition has multipolarity M1, a spin and parity of 1- was assigned to the 649.6 keV excited state of ^{206}Tl. The results of calculations of the alpha branching to the 649.6 keV excited state of ^{206}Tl are shown in Tables 22 and 23. The predominate configuration in the wave function for this excited state appears to be $(d\frac{3}{2}\ p\frac{1}{2};\ 1^-)$.

The fifth excited state of ^{206}Tl observed in this work had an excitation energy of 801.1 ± .3 keV. Alpha decay of ^{210m}Bi to this excited state of ^{206}Tl was observed in alpha singles spectra with an energy 4.420 ± .001 MeV and a branching ratio of 0.29 ± .03. Measurements of the alpha branching ratio using alpha-gamma coincidence data gave a somewhat lower value of 0.21 ± .04%. The 4.420 MeV alpha was observed in coincidence with the 266 keV and 636 keV gammas. These two gammas were also observed in coincidence with each other indicating that the 801.1 keV excited state of ^{206}Tl gamma decays to the 265.6 keV excited state of ^{206}Tl.

Decay of the 801.1 keV excited state to the 634.2 keV excited state by the emission of a 168 keV gamma is predicted to occur using the Weiskopf formula at a rate 32 times smaller than the decay rate to the 265.6 keV excited state, but a 168 keV gamma was not seen in this work. A lower limit on the ratio of 535 keV to 168 keV gammas was measured as 90. This might suggest that these transitions are E2 instead of M1. The calculated ratio between two E2 transitions with energies of 535 keV

and 168 keV is 324.

The only indication of the spin of the 801.1 keV excited state of ^{206}Tl in this work was that the decay of the 801.1 keV excited state to the 304.6 keV excited state with spin and parity 1- was not observed. If the spin of the 801.1 keV excited state is >2 then the decay to 2- states would be much faster than to 1- states because it would involve a lower order multipolarity gamma transition. If the spin of the 801.1 keV excited state is 3 as indicated by references 52 and 53 based on studies of, respectively, the ^{207}Pb (t,α)^{206}Tl and ^{208}Pb(d,α)^{206}Tl reactions, then the decay to the 265.6 keV 2- excited state would involved as the lowest order multipolarity M1 while decay to the 304.6 keV 1- excited state would involve as the lowest multipolarity E2.

Calculations of the alpha branching ratio to the 801.1 keV excited state are shown in Tables 22 and 23. Calculations using the configuration $(s_{\frac{1}{2}}\ f_{\frac{5}{2}};\ 3^-)$ gave values that were too low whereas calculations using the configuration $(s_{\frac{1}{2}}\ f_{\frac{7}{2}};\ 3^-)$ gave values that were too high.

Alpha decay to a sixth excited state of ^{206}Tl was observed in the alpha singles spectrum of ^{210m}Bi with an energy of 4.260 ± .006 MeV and a branching ratio of 0.012 ± .001%. In the alpha-gamma coincidence data a peak was seen involving a 4.268 ± .003 MeV alpha and 686 ± 1 keV gamma which corresponded to an alpha branching ratio of .006 ± .001%.

The excitation energy for this state calculated from the alpha energy 4.268 MeV was 957 ± 6 keV. Assuming that the 686 keV gamma is produced by the decay of this excited state to the 265.6 keV excited state, the energy of this state was calculated as 952 ± 1 keV.

The 686 keV gamma was seen in the gamma singles spectrum of ^{210m}Bi with an intensity of .012 ± .002%. By comparing this intensity to the

intensity of the 649.6 keV gamma the alpha branching ratio to the 952 keV excited state was calculated as .010 ± .002%.

If the spin and parity of the 952 keV excited state is 4- as suggested by reference 52, then it might be expected to decay primarily to the 801.1 keV 3- level by a 151 keV M1 transition instead of by the observed 686 keV gamma which would have a multipolarity of E2. The ratio of the 151 keV M1 transition rate to the 686 E2 transition rate calculated using the Weiskopf equations is 26. Neither a 151 keV gamma or the 535 keV gamma resulting from the subsequent decay of the 801.1 keV excited state were observed in coincidence with the 4.268 MeV alpha.

The results of calculations of the alpha branching ratio to the 952 keV excited state of ^{206}Tl are shown in Table 23.

In alpha-gamma coincidence measurements a coincidence was observed involving a 4.230 ± .008 MeV alpha and a 734 ± 2 keV gamma. The excitation energy of the ^{206}Tl excited state calculated using the alpha decay energy was 996 ± 8 keV. The 734 keV gamma is produced by the transition from this excited state to the 265.6 keV excited state. The excitation energy of the state populated by the 4.230 MeV alpha was calculated as 1000 ± 2 keV by adding the 734 keV gamma energy to the 265.6 keV excitation energy of the first excited state of ^{206}Tl.

The spin and parity assigned to this excited state by references 52 and 53 was 2-. The observations of this work do not dispute this assignment.

The calculational results for this excited state are shown in Table 23.

The highest excited state of ^{206}Tl observed in this work was seen

only in alpha-gamma coincidence measurements. An alpha with an energy of 4.100 ± .008 MeV was observed in coincidence with gammas with energies 457,536,650, and 1120 keV. The excitation energy of the ^{206}Tl state populated by the 4.100 MeV alpha was calculated as 1128 ± 8 keV using the alpha energy. If the 1120 ± 2 keV gamma is the transition of this excited state to the ^{206}Tl ground state then the excitation energy is 1120 ± 2 keV.

The decay of the 1120 keV excited state directly to the 649.6 keV excited state by the emission of a 470 keV gamma was not observed indicating that this transition must proceed through an excited state of ^{206}Tl not observed in this work.

The strong decay of this excited state to the ground state of ^{206}Tl indicates that the spin and parity of the state is 1- so that the 1120 keV gamma has a lowest order multipolarity of M1.

The results of calculations of the alpha branching to this excited state are shown in Table 23.

Appendix A. Factorization of a four nucleon wave function from the wave function for ^{211}Po

The wave function of ^{211}Po was expressed as a three nucleon wave function coupled to a ^{208}Pb core wave function. The ^{208}Pb core wave function was then expressed as a neutron coupled to a ^{207}Pb core as shown below.

$$| {}^{211}\text{Po};\ J\rangle = \left\{\left[| {}^{207}\text{Pb};\ J'\rangle \ | \ n';\ J'\rangle\ (0)\right]\left[| \ n;\ j\rangle \ | \ p^2;\text{JPP}\rangle\ (J)\right]J\right\}$$

where

$| {}^{211}\text{Po};\ J\rangle$ is a ^{211}Po shell model wave function with spin J

$| {}^{207}\text{Po};\ J'\rangle$ is a ^{207}Pb shell model wave function with spin J'

$| n';\ J'\rangle$

and $| n;\ J\rangle$ are shell model neutron wave functions with spin J' and J, respectively

$| p^2;\ \text{JPP}\rangle$ is a shell model wave function for two protons coupled to a spin JPP

The brackets indicate the order in which the angular momentum couplings should be performed.

The order of the angular momentum couplings was changed by using the Racah W function[36] as shown below.

$$| {}^{211}\text{Po};\ J\rangle = \sum_L (2L+1)^{\frac{1}{2}}\ W(J\ J'\ J\ J';\ LJ)$$
$$\left\{\left[| \ {}^{207}\text{Pb};\ J'\rangle\right]\left[\left(| \ n';\ J'\rangle\right)\left(| \ n;\ j\rangle \ | \ p^2;\ \text{JPP}\rangle\ (J)\right)(L)\right]J\right\}$$

A second reordering of the angular momentum couplings, this time within the four nucleon wave function, produced the form for the ^{211}Po wave function needed for alpha decay calculations.

$$|\,^{211}\mathrm{Po};\ J\rangle = \sum_{L} (2L+1)^{\frac{1}{2}}\, W(J\ J'\ J\ J';\ L0)$$

$$\left\{\left[|\,^{207}\mathrm{Pb};\ J'\rangle\right] \sum_{JNN} (2J+1)^{\frac{1}{2}}\ (2JNN+1)^{\frac{1}{2}}\, W(J'jL\ JPP;\ JNN\ J)\right.$$

$$\left.\left[\left(|\ n';\ J'\rangle\ |n;\ j\rangle\ (JNN)\right)\left(|\ p^2;\ JPP\rangle\right)(L)\right]\ J\right\}$$

Appendix B. Factorization of a four particle wave function from the wave function for ^{210}Bi

---

The ^{210}Bi wave function was written as a two nucleon wave function coupled to a ^{208}Pb core

$$| {}^{210}\text{Bi};\ J\rangle = \left\{ | {}^{208}\text{Pb};\ 0\rangle \ | \left[| \ n;\ j_n\rangle \ | \ p;\ j_p\rangle \ (J) \right] J \right\}$$

where

$| {}^{210}\text{Bi};\ J\rangle$ is a ^{210}Bi shell model wave function with spin J

$| {}^{208}\text{Pb};\ 0\rangle$ is a ^{208}Pb shell model wave function with spin 0

$| \ n;\ j_n\rangle$

and $| \ p;\ j_p\rangle$ are single particle shell model wave functions for a neutron and proton with spins j_n and j_p respectively

and the angular momentum coupling order is indicated by the brackets.

The ^{208}Pb core was then written in terms of a ^{206}Tl and a second two nucleon wave function, to give

$$| {}^{210}\text{Bi};\ J\rangle = \left[\left\{ \left[| \ {}^{206}\text{Tl};\ J'\rangle \right] \left[| \ n';\ j_n'\rangle \ | \ p';\ j_p'\rangle \ (J') \right] (0) \right\} \right.$$
$$\left. \left\{ | \ n;\ j_n\rangle \ | \ p;\ j_p\rangle \ (J) \right\} J \right]$$

Using Racah-W functions[36] a reordering of the angular momenta was accomplished.

$$| {}^{210}\text{Bi};\ J\rangle = \sum_L (2L+1)^{\frac{1}{2}} W(J\ J'\ J\ J';\ L0)$$
$$\left[\left\{ | \ {}^{206}\text{Tl};\ J'\rangle \right\} \left\{ \left[| \ n';\ j_n'\rangle | \ p';\ j_p'\rangle (J') \right] \left[| \ n;\ j_n\rangle | \ p;\ j_p\rangle \right] (L) \right\} J \right]$$

Then using the Fano X function the four nucleon wave function was rearranged to a form suitable for use in alpha decay constant calculations.

$$|\,^{210}\mathrm{Bi};\ J\rangle = \sum_{L} (2L+1)^{\frac{1}{2}}\, W(J\ J'\ J\ J';\ L0)$$

$$\left[\left\{|\,^{206}\mathrm{Tl};\ J'\rangle\right\}\left\{\sum_{\substack{JPP\\JNN}} (2JPP+1)^{\frac{1}{2}}\ (2JNN+1)^{\frac{1}{2}}\right.\right.$$

$$(2J+1)^{\frac{1}{2}}\ (2J'+1)^{\frac{1}{2}}\ X\ (j_n'\ j_p'\ J',\ j_n j_p J,\ JNN\ JPP\ L)$$

$$\left.\left.\left[|\ n';\ j_n'\rangle\ |\ n;\ j_n\rangle\ (JNN)\right]\left[|\ p';\ j_p'\rangle\ |\ p;\ j_p\rangle (JPP)\right](L)\right\} J\right]$$

References

1. P. Marmier and E. Sheldon, Physics of Nuclei and Particles (Academic Press, New York, 1971), pg 1261.
2. H. J. Mang, Ann. Rev. Nucl. Sci. 14, 1 (1964).
3. H. J. Mang, Phys. Rev. 119, 1069 (1960). Lawrence Radiation Laboratory Report UCRL-8931 (1959).
4. H. D. Zeh and H. J. Mang, Nucl. Phys. 29, 529 (1962).
5. H. J. Mang, Z. Physik 148, 582 (1957).
6. R. C. Lange, G. R. Hagee, and A. R. Campbell, Nucl. Phys. A133, 273 (1969).
7. L. I. Rusinov, Y. N. Andrew, S. V. Golenetskii, M. I. Kislov, and Y. I. Filimonov, JETP (Sov. Phys.) 13, 707 (1961).
8. R. J. Walen and G. Bastin-Scoffier, J. de Phys. 20, 589 (1959).
9. E. H. Spejeuski, Nucl. Phys. A100, 236 (1967).
10. G. A. Koralevand, G. E. Kocharov, Iquest. Akad. Nauk. SSSR, Ser. Fiz. 26, 235 (1962); Columbia Technical Transl. 26, 233 (1963).
11. H. B. Levy and I. Perlman, Phys. Rev. 94, 152 (1953).
12. H. M. Neuman, J. J. Howland, and I. Perlman, Phys. Rev. 77, 720 (1950).
13. S. F. Mughabghab and D. I. Garber, Neutron Cross Sections, Vol. 1, BNL-325, D180 (1973).
14. T. A. Eastwood and J. C. Roy, Can. J. Phys. 37, 815 (1959).
15. C. M. Lederer, J. M. Hollander, and I. Perlman, Table of Isotopes (John Wiley and Sons, Inc., New York, London, Sydney, 1967).
16. C. D. Hodgman, R. C. Weast, and S. M. Selby, Handbook of Chemistry and Physics, 42nd ed. (The Chemical Rubber Publishing Co., Cleveland, 1960).

17. W. W. Schulz and G. L. Richardson, Ind. Eng. Chem., Process Design Develop. 7, 149 (1968).

18. W. F. Linke, Solubilities: Inorganic and Metal Organic Compounds, 4th ed. (American Chemical Society, Washington, 1958), pg 430.

19. M. C. Michel and F. L. Reynolds, Lawrence Radiation Laboratory Report UCRL-18667, 359 (1968).

20. R. H. Escabales, C. E. Miner, R. M. Reimers, and M. C. Michel, Lawrence Radiation Laboratory Report UCRL-18667, 372 (1968).

21. O. Almin and G. Bruce, Nucl. Instr. Methods 11, 279 (1961).

22. R. Leonard, R. L. Pointing, and R. K. Sheline, Nucl. Instr. Methods 100, 459 (1972).

23. R. C. Lange and C. R.Hagee, J. Inorg. Nucl. Chem. 31, 3297 (1969).

24. P. Marmier and E. Sheldon, Physics of Nuclei and Particles (Academic Press, New York, 1971), Vol. 1, pg 420.

25. J. Dairiki, Lawrence Radiation Laboratory Report UCRL 20412, Ph. D. Thesis (1970).

26. I. Ahmad, Lawrence Radiation Laboratory Report UCRL-16888, Ph. D. Thesis (1966).

27. M. E. Rose, Internal Conversion Coefficients (Interscience Publishers, New York, 1958).

28. T. Inamura, J. Phys. Soc. Japan 24, 1 (1968).

29. H. Geiger and J. M. Nuttal, Phil. Mag. 22, 613 (1911); 23, 439 (1912).

30. G. Gamow, Z. Physik 51, 204 (1928).

31. E. U. Condon and R. W. Gurney, Nature 122, 439 (1928); Phys. Rev. 33, 127 (1929).

32. G. H. Winslow, Phys. Rev. 96, 1032 (1954).

33. J. K. Poggenburg, Lawrence Radiation Laboratory Report UCRL-16187, Ph. D. Thesis (1965).

34. H. J. Mang and J. O. Rasmussen, Kgl. Danske Videnskab. Selskab., Mat.-Fys. Skrifter 2, No. 3 (1962).

35. H. Casimir, Physica 1, 193 (1934).

36. D. M. Brink and G. R. Satchler, Angular Momentum, 2nd ed. (Clarendon Press, Oxford, 1968), pg 45.

37. M. Moshinsky, Nucl. Phys. 13, 104 (1959).

38. T. A. Brody and M. Moshinsky, Tables of Transformation Brackets for Nuclear Shell Model Calculations, 2nd ed. (Gordon and Breach Science Publishers, New York, 1967).

39. T. T. S. Kwo and G. H. Herling, Naval Research Laboratory Memorandum Report 2258 (1971).

40. H. M. Neuman and I. Perlman, Phys. Rev. 81, 958 (1951).

41. R. W. Hoff, Lawrence Radiation Laboratory Report UCRL-2325, Ph. D. Thesis (1953).

42. R. J. Walen, V. Nedovessov, G. Bastin-Scoffier, Nucl. Phys. 35, 232 (1962).

43. W. F. Davidson, C. P. Cothern, and P. D. Connor, Can. J. Phys. 45, 2295 (1967).

44. S. Guetkh, B. S. Dzhelepov, Y. V. Norseev, and V. A. Sergientko, Proc. 18th Ann. Conf. Nucl. Spectroscopy and Struct. of At. Nuclei, Riga 96 (1968).

45. N. A. Golovkov, S. Guetkh, B. S. Dzhelepov, Y. N. Norseev, V. A. Khalkin, and V. G. Chumin, Izv. Akad. Nauk. SSSR, Ser. Fiz. 33, 1622 (1969).

46. J. Bloomquist and S. Wahlborn, Arkiv f. Fys. 16, 46 (1960).

47. T. Fliessbach, Z. Physik 272, 39 (1975).

48. I. Perlman, F. Asaro, A. Ghiorso, A. Larsh, and R. Latimer, Phys. Rev. 127, 917 (1962).

49. W. H. Zoller and W. B. Walters, J. Inorg. Nucl. Chem. 32, 2465 (1970).

50. G. A. Bartholomew, E. D. Earle and M. A. Lone, Bull. Am. Phys. Soc. 15, No. 4, 550, EG11 (1970).

51. J. R. Erskine, Phys. Rev. 138, B851 (1965).

52. M. B. Lewis and U. U. Paehneck, Phys. Rev. C 1, 1577 (1970).

53. P. D. Barnes, E. R. Flynn, G. J. Igo, and D. D. Armstrong, Phys. Rev. C 1, 228 (1970).

54. C. J. Cussens, G. K. Rochester, and K. F. Smith, J. Phys. A (London) 2, 658 (1969).